

# $T_{1\rho}$ magnetic resonance: basic physics principles and applications in knee and intervertebral disc imaging

Yi-Xiáng J. Wáng<sup>1</sup>, Qinwei Zhang<sup>2</sup>, Xiaojuan Li<sup>3</sup>, Weitian Chen<sup>1</sup>, Anil Ahuja<sup>1</sup>, Jing Yuan<sup>4</sup>

<sup>1</sup>Department of Imaging and Interventional Radiology, Faculty of Medicine, The Chinese University of Hong Kong, New Territories, Hong Kong SAR, China; <sup>2</sup>Department of Radiology, Academic Medical Center, Amsterdam, The Netherlands; <sup>3</sup>Department of Radiology and Biomedical Imaging, University of California, San Francisco, USA; <sup>4</sup>Medical Physics and Research Department, Hong Kong Sanatorium & Hospital, Happy Valley, Hong Kong SAR, China

Correspondence to: Dr. Yi-Xiáng J. Wáng. Department of Imaging and Interventional Radiology, Faculty of Medicine, The Chinese University of Hong Kong, New Territories, Hong Kong SAR, China. Email: yixiang\_wang@cuhk.edu.hk.

**Abstract:**  $T_{1\rho}$  relaxation time provides a new contrast mechanism that differs from  $T_1$ - and  $T_2$ -weighted contrast, and is useful to study low-frequency motional processes and chemical exchange in biological tissues.  $T_{1\rho}$  imaging can be performed in the forms of  $T_{1\rho}$ -weighted image,  $T_{1\rho}$  mapping and  $T_{1\rho}$  dispersion.  $T_{1\rho}$  imaging, particularly at low spin-lock frequency, is sensitive to  $B_0$  and  $B_1$  inhomogeneity. Various composite spin-lock pulses have been proposed to alleviate the influence of field inhomogeneity so as to reduce the banding-like spin-lock artifacts.  $T_{1\rho}$  imaging could be specific absorption rate (SAR) intensive and time consuming. Efforts to address these issues and speed-up data acquisition are being explored to facilitate wider clinical applications. This paper reviews the  $T_{1\rho}$  imaging's basic physic principles, as well as its application for cartilage imaging and intervertebral disc imaging. Compared to more established  $T_2$  relaxation time, it has been shown that  $T_{1\rho}$  provides more sensitive detection of proteoglycan (PG) loss at early stages of cartilage degeneration.  $T_{1\rho}$  has also been shown to provide more sensitive evaluation of annulus fibrosis (AF) degeneration of the discs.

**Keywords:**  $T_{1\rho}$ ; musculoskeletal system; quantitative; biomarker; osteoarthritis (OA); cartilage; intervertebral disc; degeneration

Submitted Nov 05, 2015. Accepted for publication Dec 06, 2015.

doi: 10.3978/j.issn.2223-4292.2015.12.06

View this article at: <http://dx.doi.org/10.3978/j.issn.2223-4292.2015.12.06>

## Principle of $T_{1\rho}$ MR imaging

### $T_{1\rho}$ relaxation-theory

In MRI physics, the process of radiofrequency (RF) pulse excited spins returning to their equilibrium status is called relaxation. The magnetization is realigned with the longitudinal direction as the main magnetic field  $B_0$ . Topographical images with different contrasts can be generated based on different tissue relaxation properties. Spin-lattice and spin-spin relaxations described by relaxation time of  $T_1$  and  $T_2$  are two most commonly leveraged tissue properties, resulting in  $T_1$ -weighted and  $T_2$ -weighted images respectively.

$T_{1\rho}$  (or  $T_{1\rho}$ ) relaxation time describes spin-lattice relaxation in the rotation frame at the presence of an external RF pulse in the transverse plane.  $T_{1\rho}$  relaxation was first described in 1955 (1), but has only been applied in MRI in the late 1980's providing extra tissue information beyond  $T_1$  and  $T_2$ -weighted images (2,3). In the pure spin-lattice or  $T_2$  relaxation, magnetization undergoes relaxation in the transverse plane and decays exponentially, while it experiences a slower relaxation process at the presence of the external RF pulse called spin-lock RF pulse ( $B_{SL}$ ). Being analogous to the alignment of spins along the main magnetic field of  $B_0$  in the laboratory frame, some spins revolve around the direction of  $B_{SL}$  in the rotating frame at

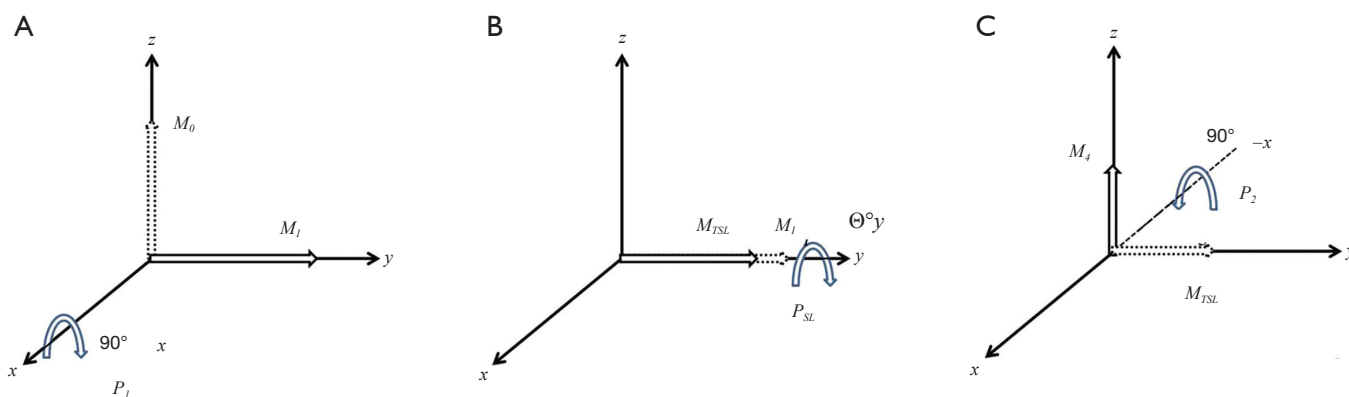


**Figure 1** Diagram of the magnetization evolution during the rotary echo spin-lock pulse cluster. (A) The initial short hard pulse was applied along the x-axis to rotate the longitudinal magnetization  $M_0$  into transverse plane along with y-axis  $M_1$ ; (B) A spin-lock pulse  $B_{SL}$  along the y-axis with duration of TSL making the magnetization rotate  $\Theta^\circ$  with frequency of FSL; (C) the final short pulse rotated the magnetization back to longitudinal direction.

the frequency determined by the *Larmor equation*,  $FSL = \gamma \cdot B_{SL}$ , where  $\gamma$  is the gyromagnetic ratio of hydrogen atom of 42.58 MHz/T and FSL is called spin-lock frequency. Note that in the case of on-resonance excitation, the influence of  $B_0$  could be neglected. The impose of  $B_{SL}$  to some degree slows the magnetization relaxation process in the transverse plane by forcing the spins process along its direction. Consequently, the relaxation time of  $T_{1\rho}$  is longer than the relaxation time of  $T_2$  for the same tissue. In addition,  $T_{1\rho}$  is positive related to the strength of  $B_{SL}$ . It is intuitive that a stronger  $B_{SL}$  is able to more efficiently “lock” the transverse spins along its direction, leading to a longer  $T_{1\rho}$  relaxation time, and that is similar to the fact that spin-lattice relaxation time  $T_1$  increases with the strength of  $B_0$ .

$T_{1\rho}$  imaging provides a viable approach to study low-frequency motional biological processes such as protein, proton exchange between water and macromolecules which may be not feasible by applying  $T_1$  or  $T_2$  MR imaging. Spin-lattice relaxation process maximizes at the spins moving at or around the Larmor frequency which is determined by the strength of  $B_0$ , e.g., about 64 MHz at 1.5T and 128 MHz at 3T, making  $T_1$  imaging difficult to directly characterize low-frequency motion atoms and molecular. Fortunately,  $T_{1\rho}$  relaxation process maximizes at FSL, which is generally in the low frequency range, i.e., several hundred Hertz, and adjustable by changing the  $B_{SL}$  strength. Therefore, the  $T_{1\rho}$  imaging can be tailored for studies of biological processes at different frequencies while taking the advantages of high field MRI scanner such as high signal to noise ratio (SNR).

### Spin-lock pulse and $T_{1\rho}$ imaging

The procedure of changing the magnetization amplitude based on the tissue  $T_{1\rho}$  value refers to  $T_{1\rho}$  weighted magnetization preparation. Like many other magnetization preparations including saturation, inversion, magnetization transfer, and chemical exchange saturation transfer,  $T_{1\rho}$ -weighted magnetization preparation itself cannot generate MR images.  $T_{1\rho}$ -weighted MR images are obtained by the subsequent acquisition sequences.

The  $T_{1\rho}$  weighted magnetization preparation pulse is often known as *spin-lock pulse* which is shown in *Figure 1*. The first short pulse  $P_1$  flips magnetization into the transverse plane along the y-axes in the rotation frame. The substantial spin-lock pulse  $P_{SL}$  is applied on the same direction with a duration of TSL and a strength of  $B_{SL}$ . The rotation angle  $\Phi_Y$  during the  $P_{SL}$  is defined by  $2\pi \cdot FSL \cdot TSL$ , where FSL is calculated by  $\gamma \cdot B_{SL}$ . A final short pulse  $P_2$  is applied opposite to  $P_1$  afterwards to return the  $T_{1\rho}$ -relaxed transverse magnetization to the original longitudinal direction.

For  $T_{1\rho}$  weighed imaging, the residual transverse magnetization is destroyed by a strong gradient crusher after the spin-lock pulse, and then a normal acquisition pulse sequence is applied for signal acquisition. Finally, a sufficiently long wait time is applied to recovery the magnetization to its equilibrium state. The block diagram for typical  $T_{1\rho}$  weighed imaging process is illustrated in *Figure 2*. In practice, other imaging module like fat suppression can be embedded into this diagram according to the specific requirements in different applications.

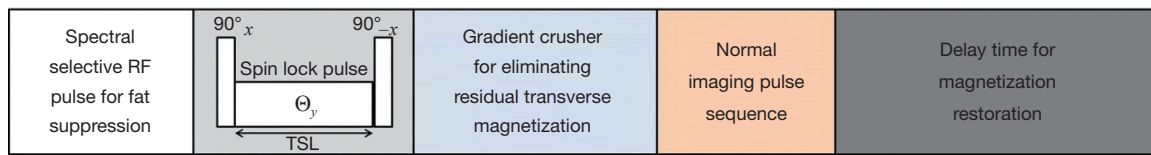


**Figure 2** Block diagram for a typical  $T_{1\rho}$  imaging MR pulse sequence. RF, radiofrequency.

### $T_{1\rho}$ weighted contrast, $T_{1\rho}$ mapping and $T_{1\rho}$ dispersion

$T_{1\rho}$  MR imaging is normally utilized in three forms. They are  $T_{1\rho}$  weighted contrast imaging,  $T_{1\rho}$  mapping and  $T_{1\rho}$  dispersion imaging.

$T_{1\rho}$  weighted contrast imaging is the basic form. This is mostly done by applying a spin-locking pulse prior to imaging, allowing adequate time for  $T_{1\rho}$  relaxation to occur, and then “storing” this  $T_{1\rho}$  prepared magnetization along the longitudinal direction.  $T_{1\rho}$  weighted contrast imaging involves only a single spin-lock time at a certain spin-lock frequency to generate an appropriate  $T_{1\rho}$  weighted contrast level.

$T_{1\rho}$  mapping is the most common form of  $T_{1\rho}$  imaging and has been most intensively used for various applications.  $T_{1\rho}$  mapping involves at least two, usually multiple spin-lock times at a certain spin-lock frequency to obtain a series of images with different levels of  $T_{1\rho}$  weighted contrast. Voxel-wise image intensities with different TSLs are then fitted to a mono-exponential decay mathematical model, described by Eq. [1], to calculate the voxel-wise  $T_{1\rho}$  values, which is called  $T_{1\rho}$  map (*Figure 3*).

$$S_i = S_0 e^{-TSL/T_{1\rho}} \quad [1]$$

Though the scan time of  $T_{1\rho}$  mapping is longer than  $T_{1\rho}$  weighted contrast imaging due to multiple TSLs were used,  $T_{1\rho}$  mapping gives voxel-wise  $T_{1\rho}$  values that are independent of acquisition sequence as quantitative biomarkers rather than the qualitative  $T_{1\rho}$ -weighted contrast for the better characterization of tissue properties.

$T_{1\rho}$  dispersion is the dependence of  $T_{1\rho}$  relaxation time with spin-lock field strength ( $B_{SL}$ ), or spin-lock frequency (FSL). Therefore,  $T_{1\rho}$  dispersion imaging usually involves  $T_{1\rho}$  quantification or mapping for at least two spin-lock frequencies. Because  $T_{1\rho}$  relaxation is sensitive to the low-frequency motional processes around or at spin-lock frequency,  $T_{1\rho}$  dispersion which is also a tissue property provides a representation of the tissue at low frequencies and reflects useful information like protein content, composition of tissue and proton exchange between water and macromolecules. The simplest  $T_{1\rho}$  dispersion imaging

is performed with two FSLs  $T_{1\rho}$  dispersion factor. The ratio of  $T_{1\rho}$  value at low and high FSL was assessed for quantification purpose (4,5).

### Techniques of $T_{1\rho}$ MR imaging

#### Design of spin-lock RF pulse

Theoretically, the magnetization along the spin-lock pulse field direction decays mono-exponentially with regard to spin-lock time TSL at the rate of  $1/T_{1\rho}$ . However, in practice, the actual spin-lock pulse field direction and strength could be obscured by the presence of  $B_0$  and  $B_1$  field inhomogeneities due either to the imperfection of MRI hardware or to the susceptibilities and heterogeneities of the imaged subject. In the presence of  $B_0$  and  $B_1$  field inhomogeneities, the effective spin-lock field direction and strength may be considerably deviated from the nominal spin-lock direction and strength, leading to the poor alignment of the magnetization along the desired spin-lock direction as well as the complicated magnetization evolution rather than the ideal mono-exponential decay along the nominal spin-lock direction.  $B_1$  inhomogeneities lead to the deviation of true spin-lock frequency from the nominal spin-lock frequency. In the presence of  $B_0$  inhomogeneities, the magnetization nutates about the effective spin-lock field direction indicated in *Figure 4*, deviated from Z direction with an angle  $\theta = \tan^{-1}(\Delta\omega_1/\Delta\omega_0) = \tan^{-1}(FSL/\gamma\Delta B_0)$ . The effective spin-lock field strength is calculated as  $\Delta\omega_{\text{eff}} = (\Delta\omega_0^2 + \Delta\omega_1^2)^{1/2}$ . This poor alignment and the complicated magnetization evolution are finally presented in the form of banding-like artifacts on  $T_{1\rho}$ -weighted images and also result in the errors of  $T_{1\rho}$  quantification using the traditional mono-exponential decay model. As seen from *Figure 4*, a simple solution to reduce the influence of  $B_0$  inhomogeneity is to use a spin-lock pulse with strong spin-lock field strength and large FSL so that  $\theta$  approaches  $90^\circ$  and  $\Delta\omega_{\text{eff}} \approx \Delta\omega_1$ . However, this is restricted by the scanner hardware performance as well as the regulation of specific absorption rate (SAR) on human scan.  $B_0$  shimming and  $B_1$  calibration are also helpful but often not sufficient to

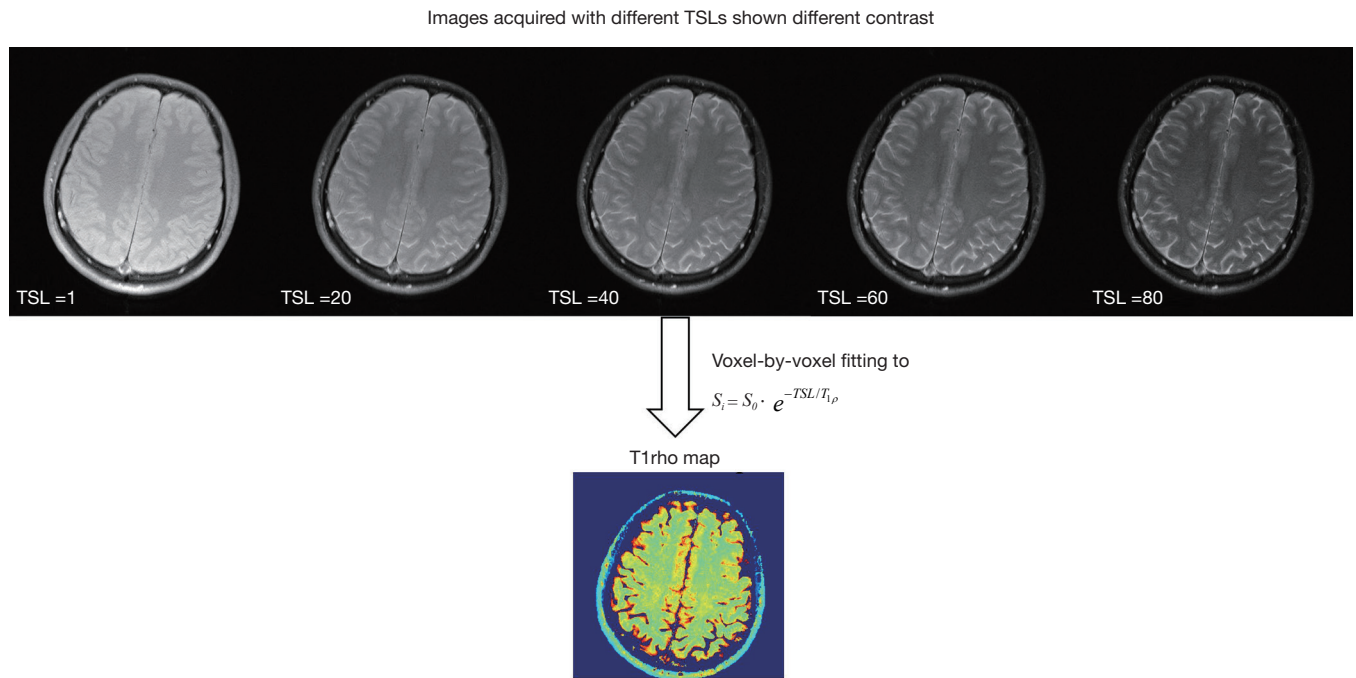


**Figure 3** The illustration of  $T_{1\rho}$  mapping from a series of images with different  $T_{1\rho}$  contrast weightings, acquired with different spin-lock times (TSLs). Note that some voxels are missing in the  $T_{1\rho}$  map due to the poor goodness-of-fit to the mono-exponential decay model.

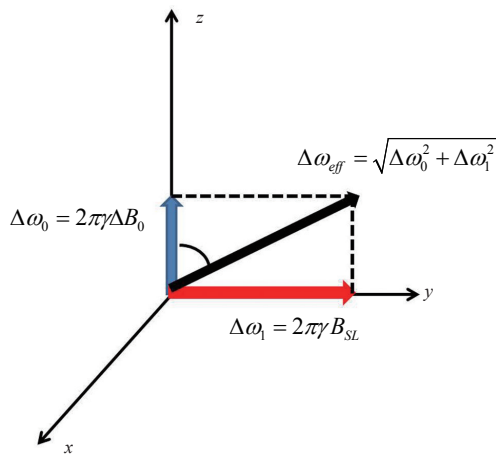


**Figure 4** Illustration of the effective spin-lock strength and direction in the rotating frame with the influence of  $B_0$  inhomogeneity.

alleviate the banding artifact. Therefore, the improved design of spin-lock RF pulse is vital to the  $T_{1\rho}$ -weighted image quality and the accurate quantification of  $T_{1\rho}$  relaxation time.

To precisely trace the magnetization evolution at each

time point during a SL pulse, full Bloch analysis is necessary but too complicated. To simplify the analysis while maintain the acceptable accuracy, the transient relaxation effect is usually neglected. As such, the magnetization evolution can be conveniently traced by the multiplication of a series of rotation and relaxation matrices to present each RF component in the cluster of a composite spin-lock pulse. An instantaneous RF pulse is represented in the form of matrix notation  $R_\phi(\phi)$ , where  $R$  denotes a rotation matrix,  $\phi$  is the pulse field orientation and  $\phi$  is the pulse flip angle. The magnetization evolution under an RF pulse could be generally expressed by  $M_{t1} = R_\phi(\phi)M_{t0}$ , where  $M_{t0}$  and  $M_{t1}$  denote the magnetization before and after the pulse excitation, respectively. The basic rotation matrices that rotate magnetization about the x, y, or z axis by an angle  $\phi$ , in three dimensions, are expressed respectively as Eq. [2]:

$$R_x(\phi) = \begin{bmatrix} 1 & 0 & 0 \\ 0 & \cos \phi & \sin \phi \\ 0 & -\sin \phi & \cos \phi \end{bmatrix}; R_y(\phi) = \begin{bmatrix} \cos \phi & 0 & -\sin \phi \\ 0 & 1 & 0 \\ \sin \phi & 0 & \cos \phi \end{bmatrix};$$

$$R_z(\phi) = \begin{bmatrix} \cos \phi & \sin \phi & 0 \\ -\sin \phi & \cos \phi & 0 \\ 0 & 0 & 1 \end{bmatrix} \quad [2]$$

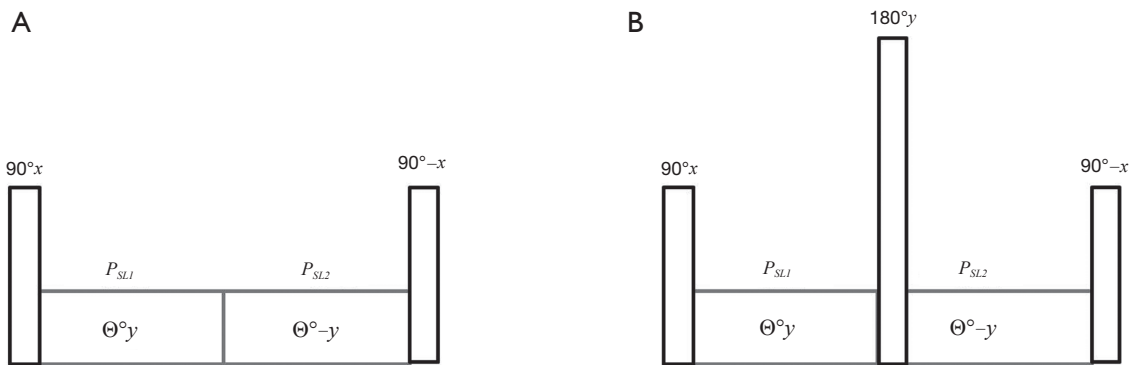


**Figure 5** MR sequence diagram. (A) Structure of a rotary echo spin-lock pulse. Spin-lock section is divided into two segments ( $P_{SL1}$  and  $P_{SL2}$ ) with the equal duration but the opposed phase; (B) structure of a composite spin-lock pulse insensitive to  $B_0$  and  $B_1$  inhomogeneity. An  $180^\circ$  refocusing pulse is inserted between the two rotary-echo spin-lock pulse segments of  $P_{SL1}$  and  $P_{SL2}$ .

Note that each of these basic magnetization vectors rotates clockwise about the axis, and the coordinate system is right-handed. The spin-lock relaxation matrix under a spin-lock pulse with duration  $T$  is given by Eq. [3], assuming spin-lock pulse is along  $y$  direction:

$$E_\rho(T) = \begin{bmatrix} e^{-T/T_{2\rho}} & 0 & 0 \\ 0 & e^{-T/T_{1\rho}} & 0 \\ 0 & 0 & e^{-T/T_{2\rho}} \end{bmatrix} = \begin{bmatrix} E_{2\rho}(T) & 0 & 0 \\ 0 & E_{1\rho}(T) & 0 \\ 0 & 0 & E_{2\rho}(T) \end{bmatrix} \quad [3]$$

Note that  $T_{2\rho}$  is the decay rate of the magnetization perpendicular to the spin lock pulse.

**Normal spin-lock pulse**

Assuming the flip angle of  $\beta$  for the tip-down pulse  $P_1$  and the tip-up pulse  $P_2$ , and  $\alpha$  for the spin-lock component SL,  $\alpha=2\pi \cdot FSL \cdot TSL$  for a given spin-lock frequency FSL, the magnetization evolution is expressed in Eq. [4]:

$$M(TSL) = R_x(\beta) \cdot R_y(\alpha) \cdot E_\rho(TSL) \cdot R_x(\beta) \cdot M(t_0) \quad [4]$$

where  $M(t_0) = [0 \quad 0 \quad M_0]^T$

Since  $P_1$  and  $P_2$  usually have much shorter duration than SL, the relaxation during  $P_1$  and  $P_2$  is negligible. By substituting Eq. [2] and Eq. [3] into Eq. [4], It is easily derived the final longitudinal magnetization  $M_z$  as given by (6).

$$M_z = (\sin^2 \beta \cdot e^{-TSL/T_{1\rho}} + \cos^2 \beta \cdot \cos \alpha \cdot e^{-TSL/T_{2\rho}}) M_0 \quad [5]$$

According to Eq. [5],  $M_z$  follows an exponential decay as long as  $\beta$  equals to  $\pi/2$  or  $90^\circ$ . In the presence of  $B_1$  inhomogeneities and  $\beta$  no longer equals to  $\pi/2$ ,  $M_z$  shows

a composite function to many factors of  $T_{1\rho}$ ,  $T_{2\rho}$  and  $\alpha$ , reflected in the image as banding artifact. Because  $\alpha$  is dependent on both TSL and FSL, the location distribution of artifacts varies with TSL and FSL as well.

**Rotary echo spin-lock pulse**

To compensate for artifacts caused by  $B_1$  inhomogeneity, a rotary echo spin-lock pulse (Figure 5A) was proposed (6). This rotary echo SL pulse is divided into two segments (SL1 and SL2 in Figure 5A) with the equal duration but the opposed phase, and effectively eliminates the rotation spin-lock phase accumulation.

The magnetization evolution under the application of a rotary echo spin-lock pulse can be expressed by Eq. [6]:

$$M(TSL) = R_x(\beta) \cdot R_y(\alpha) \cdot E_\rho(TSL/2) \cdot R_y(\alpha) \cdot E_\rho(TSL/2) \cdot R_x(\beta) \cdot M(t_0) \quad [6]$$

Note that here  $\alpha=2\pi \cdot FSL \cdot (TSL/2)$ . The final longitudinal magnetization  $M_z$  is derived as:

$$M_z = (\sin^2 \beta \cdot e^{-TSL/T_{1\rho}} + \cos^2 \beta \cdot e^{-TSL/T_{2\rho}}) M_0 \quad [7]$$

Comparing Eq. [5] and Eq. [7], the term of  $\cos \alpha$  has been completely eliminated in Eq. [7] so  $M_z$  no longer shows TSL- or FSL-dependent artifact distribution. However, it is worth pointing out that rotary echo pulse could still show some artifacts when  $\beta$  does not equals to  $\pi/2$ . Meanwhile,  $M_z$  does not show pure  $T_{1\rho}$ -weighted contrast and may contaminated by  $T_{2\rho}$ -weighted contrast in the presence of  $B_1$  inhomogeneity.

In the presence of  $B_0$  inhomogeneities, the magnetization evolution could also be traced quantitatively by Eq. [8] (7):

$$\begin{aligned}
 M(TSL) &= R_x(\beta) \cdot R_z(\alpha) E_\rho(TSL/2) \cdot R_z(\alpha) E_\rho(TSL/2) \cdot R_x(\beta) \cdot M(t_0) \\
 &= R_x(\beta) \cdot R_x(-\theta) R_z(\alpha) E_\rho(TSL/2) R_x(\theta) \cdot \\
 &\quad R_x(\theta) R_z(\alpha) E_\rho(TSL/2) R_x(-\theta) \cdot R_x(\beta) \cdot M(t_0)
 \end{aligned} \tag{8}$$

where  $\theta$  is the direction of the effective spin-lock field as shown in *Figure 4*. The final longitudinal magnetization  $M_z$  is given by:

$$\begin{aligned}
 M_z &= [e^{-TSL/T_{2\rho}} (\cos^2 \beta - \cos^2 \theta) (\sin^2 \alpha - \cos^2 \alpha \cos 2\theta) \\
 &\quad + e^{-TSL/2T_{1\rho}} e^{-TSL/2T_{2\rho}} \cos \alpha \sin^2 2\theta \\
 &\quad + e^{-TSL/T_{1\rho}} (\cos^2 \beta - \sin^2 \theta) \cos 2\theta] \cdot M_0
 \end{aligned} \tag{9}$$

Eq. [9] shows that the resultant longitudinal magnetization by a rotary echo SL pulse in the presence of  $B_0$  inhomogeneity does not show a pure  $T_{1\rho}$  contrast, but a very complicated composite contrast dependent on many factors, including  $T_{1\rho}$ ,  $T_{2\rho}$ ,  $B_0$  inhomogeneity, TSL and FSL. Although complicated, Eq. [9] provides a possible means to simultaneously quantify  $T_{1\rho}$ ,  $T_{2\rho}$  and  $B_0$  inhomogeneity even in the presence of banding-artifacts, particularly at low spin-lock frequencies (7).

### $B_1$ and $B_0$ insensitive composite spin-lock pulse

Rotary echo pulse is still susceptible to  $B_0$  inhomogeneity. Witschey *et al.* (8) proposed new  $B_1$  and  $B_0$  insensitive composite spin-lock pulses to further reduce the sensitivity of rotary echo spin-lock pulses to  $B_0$  inhomogeneities by inserting an  $180^\circ$  refocusing pulse between the two rotary-echo spin-lock pulse segments of SL1 and SL2 (*Figure 5B*). This  $180^\circ$  refocusing pulse works just similar to the refocusing pulse used in the normal spin-echo acquisition pulse sequences. The spins nutating about the effective spin-lock field direction at the first spin-echo pulse section SL1 is reversed and then return back to the original position after processing about the effective spin-lock field direction at the second spin-lock section. The analytical expression of the magnetization under this  $B_1$  and  $B_0$  insensitive composite spin-lock pulse could be derived as:

$$\begin{aligned}
 M_z &= [e^{-TSL/T_{2\rho}} (\cos^2 \beta - \cos^2 \theta) \\
 &\quad \cdot (\sin^2 \alpha \cos 2\beta - \cos^2 \alpha \cos^2 \theta + \cos 2\beta \cos^2 \alpha \sin^2 \theta) \\
 &\quad + 0.5 \cdot e^{-TSL/2T_{1\rho}} e^{-TSL/2T_{2\rho}} (1 + \cos 2\beta) \\
 &\quad \cdot (\cos \alpha \sin^2 2\theta + 2 \sin \alpha \cos \theta - 2 \cos 2\beta \sin \alpha \cos \theta) \\
 &\quad + e^{-TSL/T_{1\rho}} (\cos^2 \beta - \sin^2 \theta) (\cos^2 \theta \cos 2\beta - \sin^2 \theta)] \cdot M_0
 \end{aligned} \tag{10}$$

The detail derivation is neglected here. In Eq. [10], the flip angle of the refocusing pulse is written as  $2\beta$ . If  $\beta=90^\circ$ , Eq. [10] is simplified exactly as Eq. [7].

Another revision of this  $B_1$  and  $B_0$  insensitive composite spin-lock pulse is to change the direction of the tip-up

pulse P2 from  $-x$  to  $x$  (8) (*Figure 6*). The purpose of this alternation is to compensate for the imperfect flip angle  $\beta$  and make it more robust to  $B_1$  inhomogeneity.

### Dixon's composite spin-lock pulse and phase cycling

In 1996, Dixon *et al.* proposed a composite spin-lock pulse in the form of  $90(y)-135(x)-360(x,SL)-135(x)-90(-y)$  for myocardial suppression. This composite pulse is tolerant to shimming and frequency errors for the cases of small off-resonance. Meanwhile, the strength and duration of each section in this composite pulse are required to meet some particular quantitative relationship. Actually, the magnetization evolution under Dixon's composite spin-lock pulse could also be calculated through the approach of multiplication of a series of rotation and relaxation matrices as used above. The result suggests that the effectiveness and robustness may be restricted in practice if the  $B_0$  or  $B_1$  inhomogeneity is relatively large and the strength and duration requirement for each pulse elements are not well fulfilled.

The idea of phase cycling has also been proposed to reduce the spin-lock artifacts by using two  $T_{1\rho}$ -weighted images. The first  $T_{1\rho}$ -weighted image is acquired using a normal spin-lock pulse and the second image is acquired using the same spin-lock pulse but with the flip angle of P2 inversed. The final image is the subtraction of the acquired two images (10). Using the theoretical analysis approach above, it can be shown that the longitudinal magnetization after this process is:

$$M_z = 2 \sin^2 \beta \cdot e^{-TSL/T_{1\rho}} M_0 \tag{11}$$

As seen from Eq. [11], phase cycling is robust to  $B_1$  inhomogeneities. Even the tip pulse flip angle  $\beta$  is not exactly  $90^\circ$ , the resulting magnetization still follows the mono-exponential decay and suffers no contamination from  $T_{2\rho}$  relaxation and the spin-lock flip angle  $\alpha$  relating to FSL and TSL. On the other hand, the disadvantage of phase cycling is also obvious. The acquisition of two images doubles the scan time.

Recently, Chen *et al.* (11) combined the Dixon's composite spin-lock pulse and phase cycling together, named phase-cycled composition spin-lock (PCC-SL), for  $B_0$  and  $B_1$  field inhomogeneity compensation, and compared the performance of PCC-SL with individual Dixon's approach, phase cycling and other composite spin-lock pulses. The results showed that PCC-SL outperformed to other approaches in artifact reduction and  $T_{1\rho}$

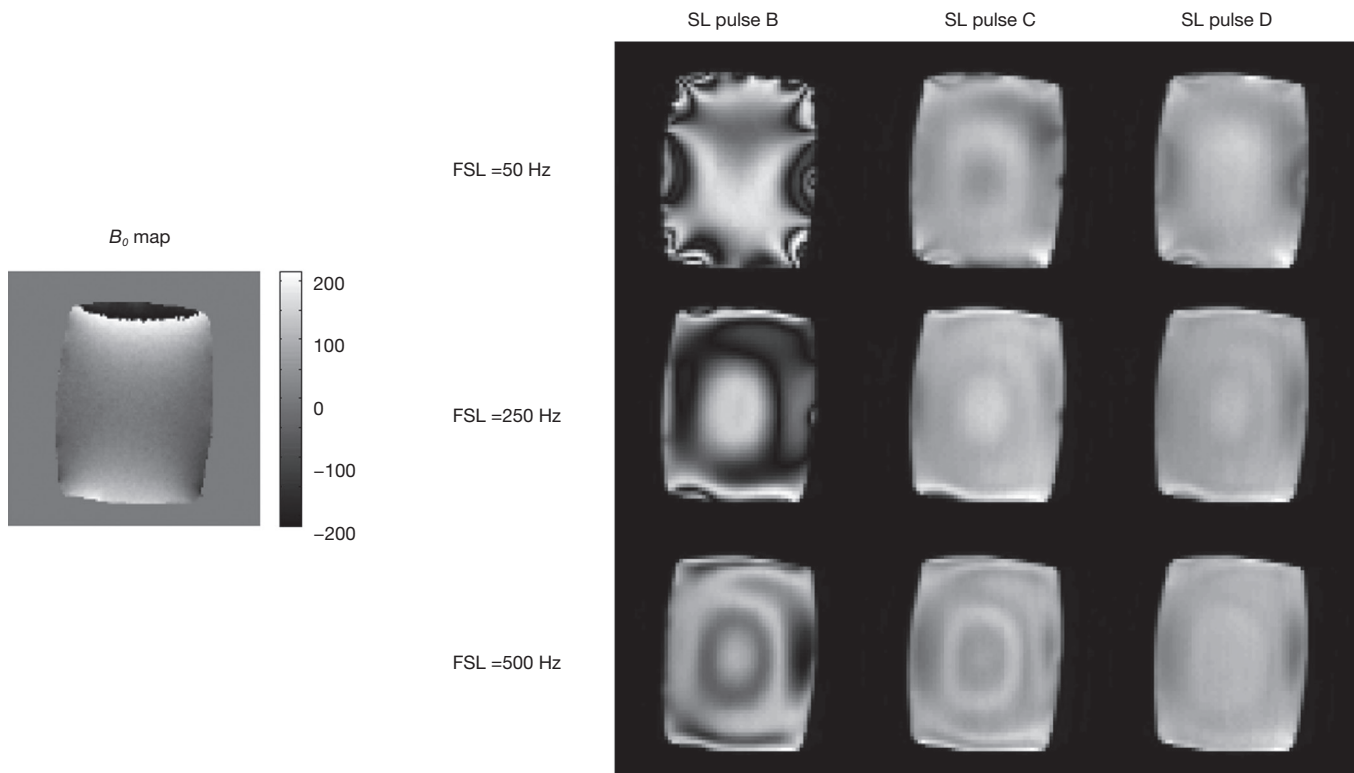


**Figure 6**  $T_{1\rho}$  weighted images obtained by using three composite spin-lock pulses to reduce the artifacts at 3 Tesla [Reprinted with permission (9)].

quantification.

In summary, many approaches have been proposed to design composite spin-lock pulses for  $T_{1\rho}$  imaging to reduce spin-lock artifact and hence more accurate  $T_{1\rho}$  quantification. Although significantly improvement compared to the traditional spin-lock pulse, the availability of these composite spin-lock pulses on clinical scanners is still limited. Meanwhile, effectiveness and robustness of these composite spin-lock pulses may still be compromised in practice and have to be further validated, in particular for the cases of long spin-lock duration, low spin-lock frequency and pronounced susceptibilities.

#### **Pulse sequences used for $T_{1\rho}$ imaging data acquisition**

The pulse sequences used for quantitative  $T_{1\rho}$  imaging usually consist of  $T_{1\rho}$  preparation followed with data acquisition. There are a number of imaging sequences which can be used to collect data after  $T_{1\rho}$  contrast is imparted into the magnetization. The signal evolution during imaging sequence may complicate the quantification

of  $T_{1\rho}$  and therefore care is needed in pulse sequence design for quantitative  $T_{1\rho}$  imaging.

Borthakur *et al.* (12) reported a 3D imaging method based on steady state spoiled gradient echo acquisition. The signal at steady state in this method can be expressed by the following equation:

$$I(TSL) = I_0 \frac{e^{(-TSL/T_{1\rho})} \{1 - e^{[-(TR-TSL)/T_1]}\}}{1 - e^{(-TSL/T_{1\rho})} e^{[-(TR-TSL)/T_1]} \cos \alpha} \sin \alpha \quad [12]$$

where  $\alpha$  is the flip angle, and TR is the repetition time. Note Eq. [12] deviates from conventional mono-exponential model used for  $T_{1\rho}$  quantification and the knowledge of  $T_1$  is needed in the model. The presence of flip angle in Eq. [12] indicates the sensitivity of this method to  $B_1$  inhomogeneity.

Li *et al.* (13) reported a 3D quantitative  $T_{1\rho}$  imaging method termed MAPSS which is based on segmented SPGR acquisition. The data is acquired during the transient signal evolution toward steady state. If the magnetization after  $T_{1\rho}$  preparation is  $M_{\text{prep}}$ , with Bloch equations, it can be shown that for segmented SPGR acquisition the transverse magnetization after the  $n$ th RF pulse is (13):

$$M_{xy}(n) = A(n)M_{prep} + B(n) \quad [13]$$

The expression of  $A(n)$  and  $B(n)$ , which are complicated functions of relaxation parameters and pulse sequence parameters, can be found in reference (13). Note the term  $B(n)$  in Eq. [13] is an additive term which causes the model deviate from mono-exponential decay. Li *et al.* (13) proposed to acquire two data sets with phase cycling of the tip-up RF pulse at the end of T1rho preparation, and form the final images by subtracting them from each other to remove  $B(n)$  term. This method makes it feasible to use simple mono-exponential decay to quantify  $T_{1\rho}$  value, however, at the cost of doubled scan time.

The magnetization after  $T_{1\rho}$  preparation can also be acquired with conventional multi-slice 2D imaging methods.  $T_1$  relaxation during imaging data acquisition can cause signal to deviate from mono-exponential model. The same phase cycling method has been reported to address this issue in multi-slice quantitative  $T_{1\rho}$  imaging (10).

Fast (or Turbo) Spin Echo (FSE or TSE) has also been reported for  $T_{1\rho}$  imaging (14,15). In FSE acquisition, when the CPMG condition is met and the crusher gradient is sufficient so that FID is eliminated,  $T_1$  recovery during the readout does not confound the relaxation profile imparted in magnetization from  $T_{1\rho}$  preparation. The point spread functions are identical for data acquired at different TSLs. Therefore, the relative image intensity at different TSLs depends only on  $T_{1\rho}$  exponential decay during T1rho prep, and no phase cycling is needed in order to use mono-exponential relaxation model, which makes FSE based  $T_{1\rho}$  imaging highly SNR efficient. The downsides of 3D  $T_{1\rho}$  imaging with FSE acquisition include the requirement of CPMG condition, increased echo time, and potential blurring from long echo train (14).

Balanced gradient echo (16) has also been reported for  $T_{1\rho}$  imaging. Instead of acquiring imaging data in steady state, signal needs to be acquired during transient stage. Otherwise, contrast loss during the transient decay can result in elevated  $T_{1\rho}$  estimation (16).

### ***Towards fast $T_{1\rho}$ imaging at high field with low SAR***

To apply  $T_{1\rho}$  imaging for clinical applications, RF energy deposition by the spin-lock pulses has to be concerned and the associating SAR has to meet the requirement of relevant safety regulations. SAR is normally defined as the amount of RF energy per unit mass per unit time deposited into the imaged subject during an imaging experiment.

For example, the U.S. Food and Drug Administration (FDA) has established guidelines to regulate the allowable maximum SAR for clinical imaging, i.e., 4 W/kg averaged over the whole body for any 15-minute period, 3 W/kg averaged over the head for any 10-minute period; or 8 W/kg in any gram of tissue in the extremities for any period of 5 minutes.

According to the SAR model proposed by Collins *et al.* in 1998 (17), SAR is proportional to the square of the RF pulse flip angle and the square of static field strength  $B_0$ . In general,  $T_{1\rho}$  imaging is SAR intensive due to the long spin-lock time and hence large flip angle. Furthermore, spin-lock pulses with strong field strength and spin-lock frequency are often preferable for the purpose of artifact reduction, which makes the SAR problem more prominent in practice, particularly for high field MRI scanners. In order to maintain the SAR within the allowable limits, acquisition TR for  $T_{1\rho}$  imaging is often significantly lengthened, resulting in a proportional increase of the total scan time and hence the reduction of patient comfort as well as the increased proneness to motion artifact.

The most straightforward and convenient method for the reduction of SAR is to reduce the spin-lock field strength or spin-lock frequency. Unfortunately, the fact is that this method is rarely used because the low spin-lock frequency also brings the severe problem of spin-lock artifact in the presence of  $B_0$  and  $B_1$  homogeneities and hinders the accurate quantification of  $T_{1\rho}$ . In this aspect, the use of various dedicated composite spin-lock pulse to reduce spin-lock artifact is beneficial for SAR reduction. Another approach is to quantify  $T_{1\rho}$  using the model different from the mono-exponential one even in the presence of artifact, if the magnetization evolution and its relationship with imaging parameters could be analytically derived (7). This approach does not require the complicated design of composite spin-lock pulses but the analytical  $T_{1\rho}$  model has to be derived individually for each kind of spin-lock pulse. Sensitivity, accuracy and precision of  $T_{1\rho}$  fitting according to these complicated models with regard to imaging parameters have to be concerned and investigated carefully to justify the fitting results.

For  $T_{1\rho}$  mapping studies in which multiple TSLs are usually applied, the reduction of the TSL number, is also an effective means to reduce the total spin-lock RF energy deposition and the total scan time, although the averaged SAR does not reduce. Theoretically, two TSLs are sufficient to calculate  $T_{1\rho}$  based on the mono-exponential model because  $T_{1\rho}$  is the only unknown parameter to be fitted.

However, the calculated  $T_{1\rho}$  may be susceptible to noise and the accuracy of  $T_{1\rho}$  calculation is much dependent on the TSL applied, true  $T_{1\rho}$  value and signal-to-noise ratio. Yuan *et al.* (18) studied the accuracy of  $T_{1\rho}$  mapping by using two TSLs through theoretical analysis and Monte Carlo simulation. Segmented  $T_{1\rho}$  acquisition could also be applied to reduce SAR for each TSL. In this approach, spin-lock pulse is not applied for each k-space line acquisition. Instead, every spin-lock pulse for  $T_{1\rho}$  preparation is followed by acquisitions of multiple k-space lines. The extreme case of segmented  $T_{1\rho}$  acquisition is the single-shot  $T_{1\rho}$  acquisition in which all k-space lines are acquired after the only one  $T_{1\rho}$  preparation.

Spin-lock RF pulse is an important source of RF energy deposition but not the only one because it has to be combined with normal acquisition pulse sequences. Therefore, other general approaches to reduce SAR could also be employed. For example, the use of partial Fourier acquisition and parallel imaging (19-21) is helpful to reduce the phase-encoding numbers and hence the number of spin-lock pulses applied. Compressed sensing reconstruction (22,23) is also beneficial and some preliminary results have been presented (24). It is well known that MR image contrast is majorly determined by the central k-space lines while the peripheral k-space lines determine the fine edge detail. Wheaton *et al.* (25) proposed a partial k-space acquisition approach in which a full power spin-lock pulse is applied to only the central phase-encode lines of k-space, while the remainder of k-space receives a low-power spin-lock pulse. SAR was reduced by 40% while the error of  $T_{1\rho}$  mapping was only 2%, as demonstrated on human brain  $T_{1\rho}$  imaging at 1.5T. For some specific applications in which only a fraction of the whole image may be interested, such as spine and cartilage  $T_{1\rho}$  imaging, reduced field-of-view (rFOV) method (26,27) could be applied to reduce the phasing encoding numbers and hence SAR and total scan time. For the application of  $T_{1\rho}$  imaging at ultra-high field strength  $B_0$  higher than 3T, the design of spin-lock pulse based on parallel excitation (28) should be promising to reduce SAR.

## Applications of $T_{1\rho}$ MR imaging

### *Applications of $T_{1\rho}$ MR imaging in articular cartilage*

During the recent years,  $T_{1\rho}$ -weighted contrast,  $T_{1\rho}$  relaxation time mapping, and  $T_{1\rho}$  dispersion have been extensively studied, covering various organs and a wide

range of disease processes, including brain (29-38), heart (39,40), liver (41-45), muscle (46,47) cancer (4,48), and joint cartilage (39), intervertebral discs (49).  $T_{1\rho}$  MR imaging is a relative time consuming technique, imaging of joint and intervertebral disc usually benefit from is very limited physiological motion. This review primarily covers  $T_{1\rho}$  imaging's application in articular cartilage. For other musculoskeletal components, another recent review has wider coverage (50).

Osteoarthritis (OA) is a multifactorial disease characterized primarily by the progressive loss of articular cartilage. OA constitutes a significant health burden affecting more than 27 million people in US alone (51,52), and has been recognized as one of the fastest growing medical conditions world wide due to the increased prevalence of obesity and aging of society (53). The disease is characterized primarily by articular cartilage degeneration, however, cartilage loss and OA symptoms are preceded significantly by damage to the collagen-proteoglycan (PG) matrix and elevation of cartilage water content (54) (*Figure 7*).

Due to aging populations and increasing rates of obesity in the developed world, the prevalence of OA is continually increasing. Decreasing the societal and patient burden of this disease motivates research in prevention, early detection of OA, and novel treatment strategies against OA. One key facet of this effort is the need to track the degradation of tissues within joints, especially cartilage. Currently, conventional imaging techniques provide accurate means to detect morphological deterioration of cartilage in the later stages of OA, but these methods are not sensitive to the subtle biochemical changes during early disease stages. During the past decade, MR techniques that quantify cartilage matrix changes have developed rapidly, with the rationale that detecting early and subtle cartilage degeneration is critical for allowing early intervention, monitoring treatments, and allowing prevention strategies for OA (55-58). Among these techniques,  $T_{1\rho}$  has gained significant attention which needs no contrast agent and detects early changes in cartilage matrix with a high sensitivity to loss of PG.

*In vitro* studies have evaluated the relationship between  $T_{1\rho}$  and the biochemical composition of cartilage. Early studies using bovine cartilage demonstrated a strong correlation between changes in PG and  $T_{1\rho}$  (59), and proposed  $T_{1\rho}$  as a more specific indicator of PG content than  $T_2$  relaxation in trypsinized cartilage (60). In  $T_{1\rho}$  imaging experiments, the spin-lock techniques reduce dipolar interactions and therefore reduce the dependence of

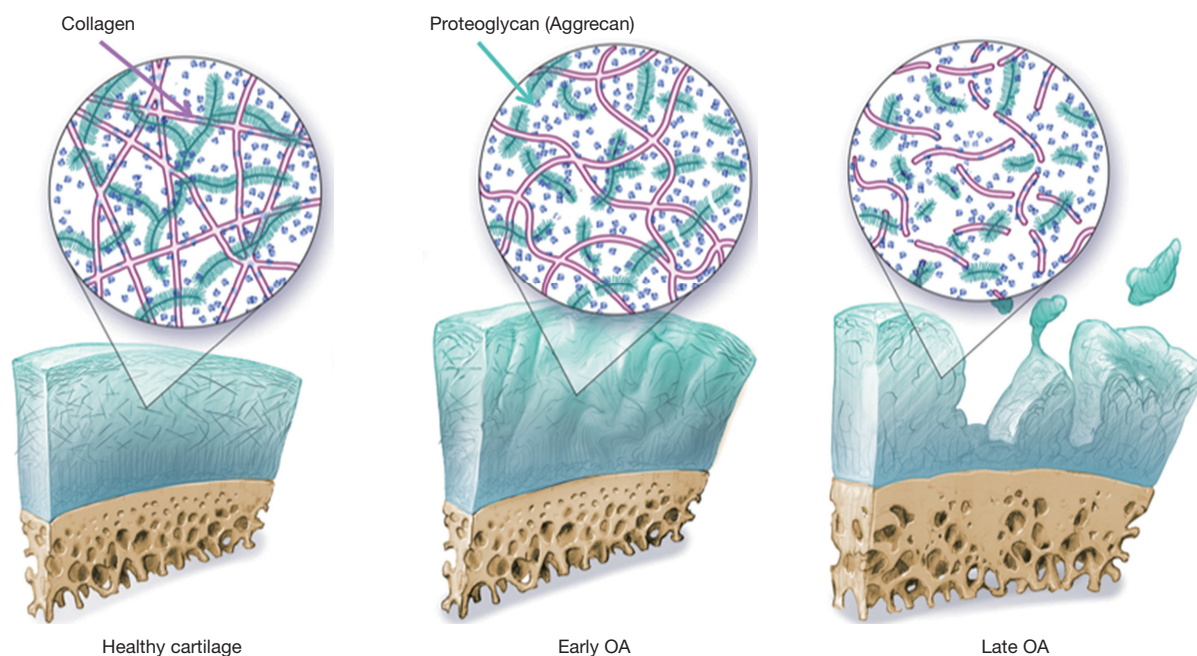


**Figure 7** Articular cartilage and degeneration during osteoarthritis (OA). Changes at early stages of OA include hydration, loss of proteoglycan (PG), thinning and loosening of collagen. Changes in late stages include further loss of PG and collagen, dehydration, extensive fibrillation and cartilage thinning, and eventually denudation of the subchondral bone [Reprinted with permission (55)].

the relaxation time constant on collagen fiber orientation in cartilage (61). This enables more sensitive and specific detection of changes in PG content using  $T_{1\rho}$  as compared to  $T_2$ , although  $T_{1\rho}$  changes in cartilage may be affected by hydration and collagen structure as well. The reduced dipolar interaction also results in less 'magic angle effect' in  $T_{1\rho}$  imaging as compared to  $T_2$  imaging. Less laminar appearance was observed in  $T_{1\rho}$ -weighted images compared to  $T_2$ -weighted images (61). Previous specimen studies reported that  $T_{1\rho}$  values at the magic angle ( $54.7^\circ$ ) were significantly higher than at other angles, but the difference was smaller than the difference in  $T_2$  values at the same angles (62). The difference was decreased with increased  $T_{1\rho}$  spin-lock frequencies and was diminished when  $T_{1\rho}$  spin-lock frequency was equal to or higher than 2K Hz (61). In OA cartilage obtained from patients who underwent total knee arthroplasty, it was demonstrated that  $T_{1\rho}$  values were correlated with clinical and histological grades of degeneration and with GAG contents (62,63). In addition to GAG concentration,  $T_{1\rho}$  has also been reported to correlate with biomechanical properties of cartilage.  $T_{1\rho}$  relaxation rate was strongly correlated with aggregate modulus and hydraulic permeability in bovine cartilage (64). Using indentation techniques, significant site-specific

correlation was observed between  $T_{1\rho}$  and the phase angle, a viscoelastic mechanical behavior of the cartilage measured by indentation, in human OA tibial specimens (65). Recent studies showed that the adiabatic and continuous wave  $T_{1\rho}$  were strongly correlated with OARSI grade and biomechanical parameters (66), and  $T_{1\rho}/T_2$  were correlated with cartilage initial elastic modulus at both 500 Hz and 1,000 Hz (67). These studies form the experimental basis for using the  $T_{1\rho}$  mapping techniques in studying cartilage pathology in OA.

The mechanism of  $T_{1\rho}$  relaxation time in biological tissues, particularly in cartilage, is not fully understood yet. Using native and immobilized protein solution, Makela *et al.* suggested that proton exchange between the protein side chain groups and bulk water contribute significantly to the  $T_{1\rho}$  relaxation (68). Based on spectroscopy experiments with peptide solutions, GAG solutions and bovine cartilage samples before and after PG degradation, Duvvuri *et al.* further suggested that in cartilage hydrogen exchange from NH and OH groups to water may dominate the low frequency (0–1.5 KHz) water  $T_{1\rho}$  dispersion (69). They speculated that increase of the low frequency correlation rate with PG loss could be the result of increased proton exchange rates. Other evidence of a proton exchange

pathway is the PH dependency of  $T_{1\rho}$  values in the ischemic rat brain tissues (70). Mlynárik *et al.* on the other hand, have suggested that the dominant relaxation mechanism in the rotating frame in cartilage at  $B_0 \leq 3T$  seems to be dipolar interaction (71). The contribution of scalar relaxation caused by proton exchange is only relevant at high fields such as 7T. Clearly, further investigations are needed to better understand this relaxation mechanism.

*In vivo*  $T_{1\rho}$  reproducibility from single site studies was reported excellent with CVs ranging from 1.7–8.7% (10,13,72). Results from multicenter studies however vary, with one study reported CV ranging 7–19% (73), while one more recent study ranging 2–6% (74). Future studies are warranted to evaluate multi-site multi-vendor variation of  $T_{1\rho}$  quantification with a clinical trial setup.  $T_{1\rho}$  values were shown to increase with ages (75) and were significantly higher in women than men in patellofemoral and lateral tibial-femur compartments in a middle-aged OA cohort (18 men, 25 women) (76). *In vivo* studies show increased cartilage  $T_{1\rho}$  values in OA subjects compared to controls (10,15,75,77–80).  $T_{1\rho}$  and  $T_2$  values in asymptomatic active healthy subjects with focal cartilage abnormalities were found to be significantly higher than those without focal lesions (75), suggesting that  $T_{1\rho}$  and  $T_2$  could be parameters suited to identify active healthy subjects at higher risk for developing cartilage pathology. In patients ( $n=20$ ) with patellar-femoral pain (PFP) but no evidence of OA, significant elevated  $T_{1\rho}$  were found in the lateral facet of patella cartilage, but no medial facet, compared to controls, and the  $T_{1\rho}$  values of PFP patients were significantly correlated with the degree of patellar tilt (81). No significant differences were noted in  $T_2$  relaxation times. Further, elevated  $T_{1\rho}$  was observed in subcompartments in OA subjects where no obvious morphologic changes were observed, suggesting the capability of  $T_{1\rho}$  in detecting very early biochemical changes within the cartilage matrix (78).  $T_{1\rho}$  measurements were reported to be superior to  $T_2$  in differentiating OA patients from healthy subjects, especially at early stages (75,78,82), potentially due to the higher sensitivity of detecting PG changes in the matrix. Elevated  $T_{1\rho}$  has been correlated with lesions identified with arthroscopy, and showed increased sensitivity and specificity of detecting cartilage damage compared to morphologic images (83–86) (Figure 8).  $T_{1\rho}$  imaging has also been applied to evaluate cartilage repair tissue after following microfracture (MFx) and mosaicplasty (MOS) cartilage resurfacing procedures, and showed preliminary results that a differentiation between different tissue types

after cartilage repair procedures was possible by applying  $T_{1\rho}$  mapping, in particular, in combination with  $T_2$  mapping (87–89).

In addition to the average values, the heterogeneity of  $T_{1\rho}$  values was evaluated using gray-level co-occurrence matrices (GLCM) (90–93). Significant increased heterogeneity of cartilage  $T_{1\rho}$  and  $T_2$  were observed in subjects with OA compared to controls, and such texture analysis showed improved group discrimination as compared to the global average (91). The pixel-by-pixel correlation between  $T_{1\rho}$  and  $T_2$  showed a large range in both controls and OA patients ( $R^2$  ranging from 0.221 to 0.763 in OA patients *vs.*  $R^2$  ranging from 0.547 to 0.726 in controls) (92). These results suggested  $T_{1\rho}$  and  $T_2$  may have different spatial distribution and provide complementary information regarding cartilage degeneration in OA (Figure 9). Combining these two parameters may improve our capability for diagnosis and staging the disease.

The relationship between cartilage degeneration and lesions of other tissues in the joint were studied using  $T_{1\rho}$  imaging.  $T_{1\rho}$  values of medial femoro-tibial cartilage were significantly higher in subjects having meniscal tears compared to subjects without a meniscal tear (94–96). These studies provided quantitative evidence linking meniscal injury to OA development.  $T_{1\rho}$  values were reported to be higher in regions overlying bone marrow edema-like lesions (BMEL) in subjects with OA and acute anterior cruciate ligament (ACL) injury (97). OA patients with BMEL showed overall higher  $T_{1\rho}$  values in cartilage compared with those who had no BMEL, suggesting BMEL may be correlated with disease severity of OA (98). Furthermore, cartilage overlying BMEL showed a significantly higher  $T_{1\rho}$  value increase from baseline to 1-year follow up compared to surrounding cartilage, suggesting BMEL is indicative of accelerated cartilage degeneration. Interestingly, no such difference was found using WORMS scoring. This result suggests that quantitative cartilage imaging, such as  $T_{1\rho}$ , may be a more sensitive indicator of cartilage degeneration than semi-quantitative scoring systems.

Previous clinical studies suggest that acute ACL injury is a risk factor for post-traumatic OA development and  $T_{1\rho}$  imaging have been applied for assessment of early cartilage damage and degeneration after ACL injury (85,97,99–103). Significant elevated cartilage  $T_{1\rho}$  values were observed after acute ACL injury (normally less than 6-month of injury and before ACL reconstruction) (97,99). The most significant  $T_{1\rho}$  elevation was normally observed in posterior lateral tibia overlying BMELs, indicating the damage to

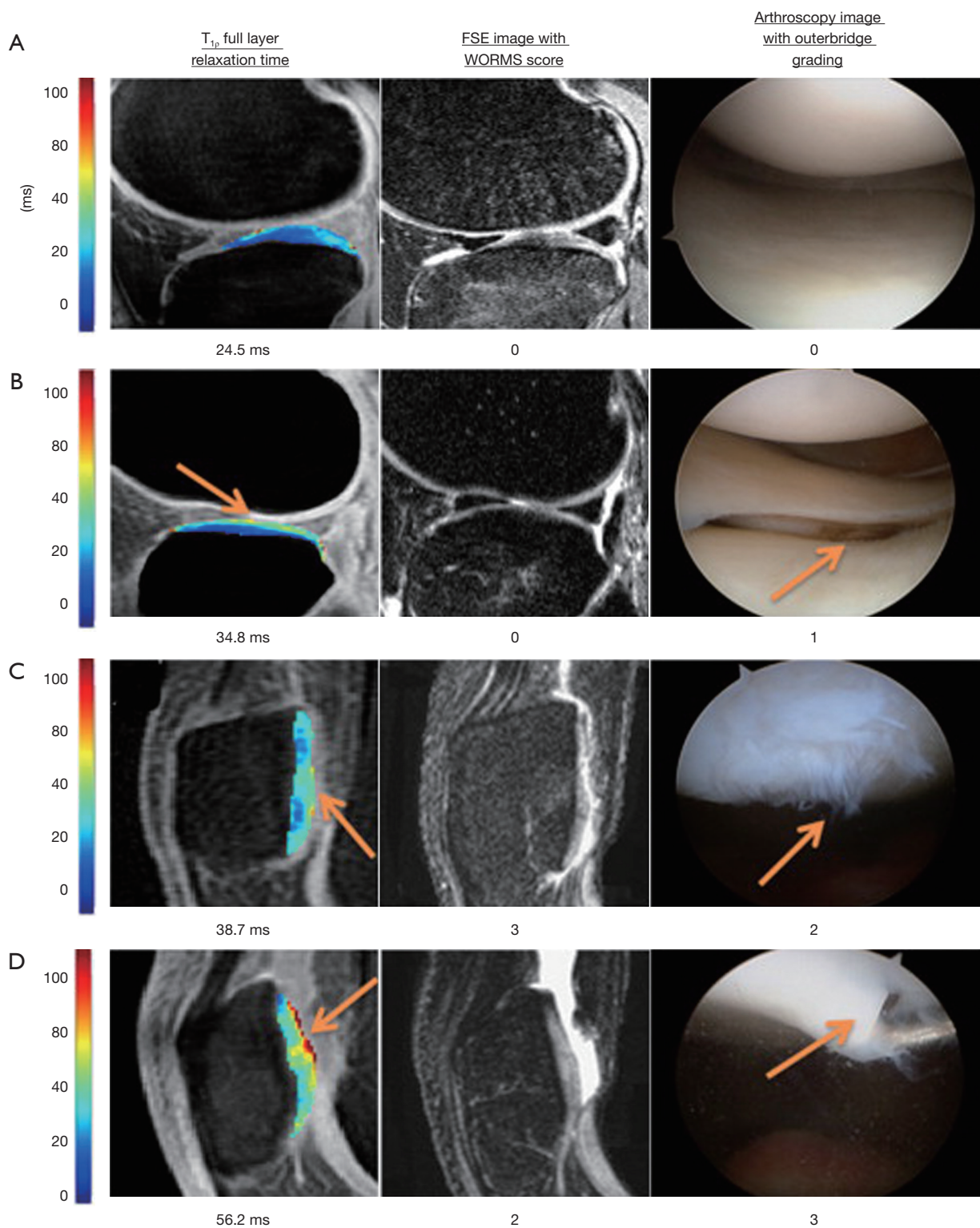


**Figure 8** Color maps of  $T_{1\rho}$  relaxation times alongside registered FSE images and arthroscopy images of the same region. Increased  $T_{1\rho}$  relaxation times are observed in conjunction with the increased Outer bridge grading of 0 to 3. Elevated  $T_{1\rho}$  values were observed in regions with arthroscopically confirmed focal lesions (as indicated by arrows) [Reprinted with permission (86)]. FSE, Fast Spin Echo.

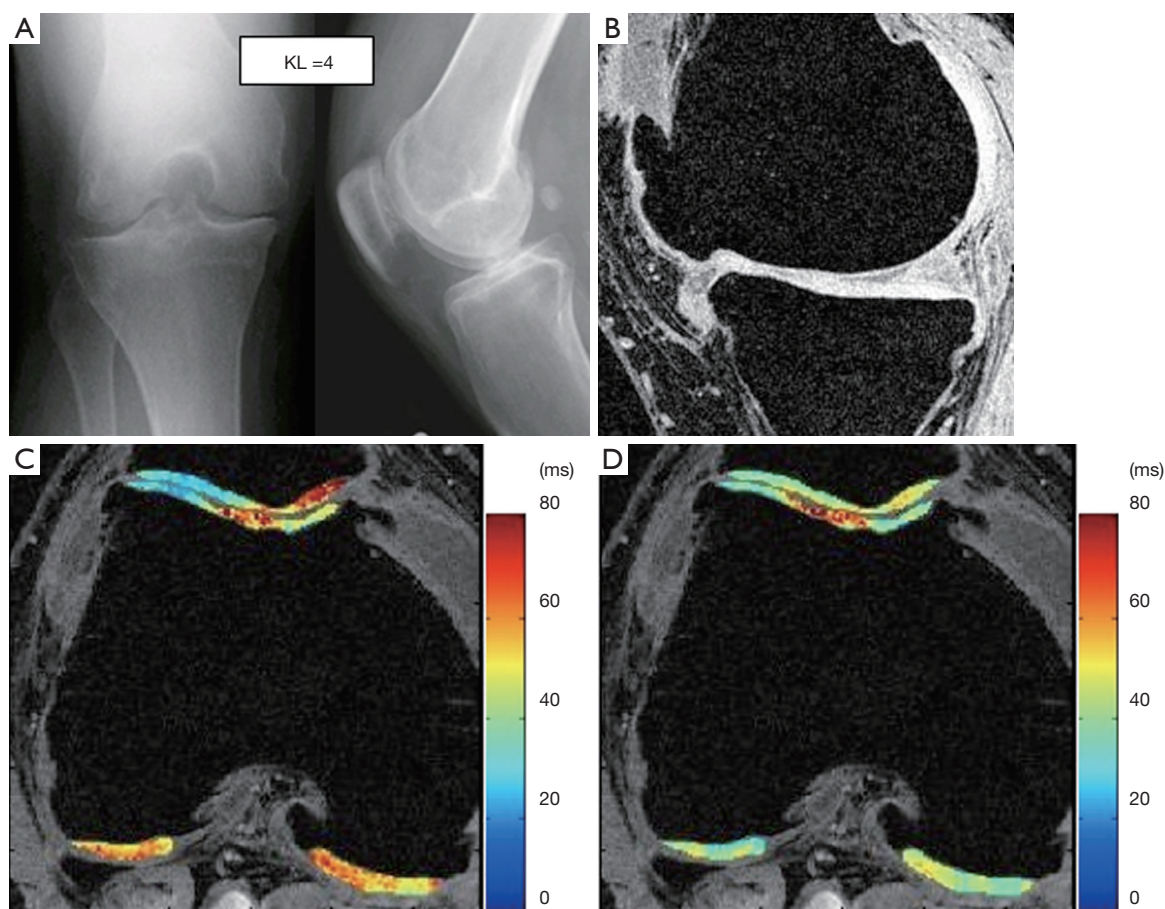


**Figure 9** Radiographs (A),  $T_1$ -weighted water excitation SPGR image (B),  $T_{1\rho}$  map (C) and  $T_2$  map (D) for a patient with advanced OA (male, 46). Based on radiographs, the patient had joint space narrowing with 1 mm in medial compartment and 3 mm in lateral compartment, and significant osteophytes in both femoro-tibial and femoro-patellar joints, resulting in a KL score as 4. In MR images, significant osteophytes were seen in both femoro-tibial and femoro-patellar joints. The cartilage had a grade 3 thinning in medial femur, medial tibia and femoro-patellar compartments, and grade 2 thinning in lateral femur and lateral tibia compartments. The average  $T_{1\rho}$  value was  $55.4 \pm 26.0$  ms and the average  $T_2$  value was  $43.8 \pm 11.1$  ms in cartilage [Reprinted with permission (78)]. OA, osteoarthritis.

cartilage during the initial injury.  $T_{1\rho}$  values in posterior lateral tibia were correlated with the volume of BMEL (97), suggesting that  $T_{1\rho}$  values in these regions may be a potential indicator of injury severity during ACL tear. After ACL reconstruction, cartilage  $T_{1\rho}$  values in posterior lateral tibia decreased compared to baseline but were still significantly higher than controls, suggesting potential irreversible damage of cartilage in these regions despite the resolution of BMEL (Figure 10). In the medial side,  $T_{1\rho}$  values were significantly higher than controls as early as 1-year after ACL reconstruction, and keep increasing over 2-year after ACL reconstruction (100,101,103). Using loaded MRI, it was recently demonstrated that the abnormal

knee kinematics including anterior tibia translation and internal rotation, is correlated with  $T_{1\rho}$  in the medial side of the ACL-reconstructed knees (104,105). Increased  $T_{1\rho}$  values in the medial side of ACL-reconstructed knees were also correlated to higher peak knee adduction moments (KAM) measured with 3D motion analysis (106). These results provide quantitative direct evidence of linking abnormal biomechanics to the joint degeneration after ACL reconstruction. Quantitative  $T_{1\rho}$  can probe these degenerations at much earlier time points than radiographs or conventional MRI.

Loading plays a critical role in the development of healthy cartilage, as well as in the progression of OA. Both

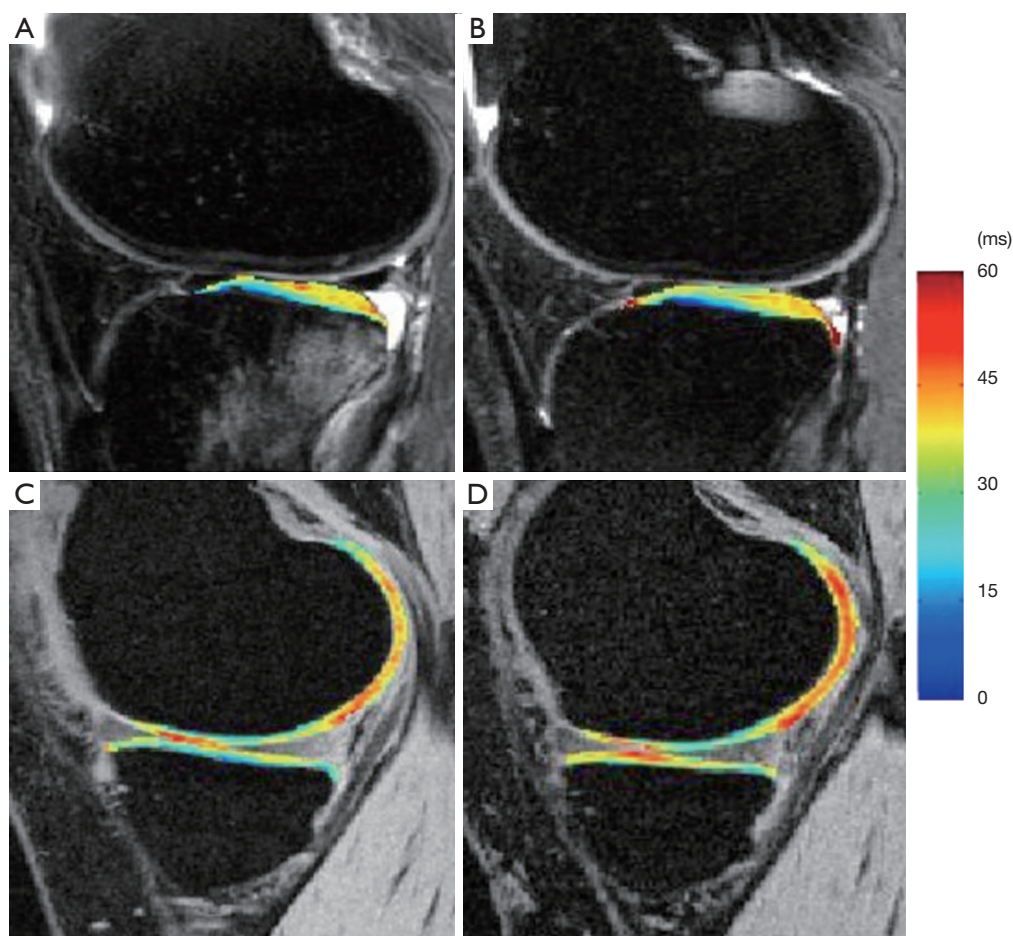


**Figure 10**  $T_{1\rho}$  maps of the lateral side (A,B) and medial side (C,D) of an ACL-injured knee at baseline (A,C) and one-year follow up (B,D).  $T_{1\rho}$  values in posterior lateral tibia were elevated significantly in ACL-injured knees at baseline and remained high at 1-year follow despite resolution of bone bruise.  $T_{1\rho}$  values in the contacting area of medial femoral condyle and medial tibia were significantly elevated in ACL-injured knees at one-year follow up [Reprinted with permission (100)]. ACL, anterior cruciate ligament.

excessive load and inadequate load have been shown to result in degenerative changes in articular cartilage (107-109).  $T_{1\rho}$  imaging provides a powerful *in vivo* tool to study cartilage responses to loading quantitatively. MRI  $T_{1\rho}$  and  $T_2$  were applied to evaluate cartilage changes in asymptomatic marathon runners (110,111). Significantly higher  $T_2$  and  $T_{1\rho}$  values were observed within 48 hours after running, although runners did not demonstrate any gross morphologic MRI changes after running a marathon (110). More interestingly, after 3 months the  $T_2$  values recovered to baseline in all compartments except for the medial femoral condyle, while  $T_{1\rho}$  values remained elevated at the 3-month follow-up MRI (110). These results suggest that while  $T_2$  may be more subjected to transient fluid shifts (in the articular cartilage and meniscus) as responses to loading,

$T_{1\rho}$  may be an indicator of early loss of PG in cartilage matrix.

Significant differences in  $T_{1\rho}$  was found in asymptomatic female collegiate athletes between impact subjects (ten basketball players) and nonimpact subjects (ten swimmers), suggesting different loading to the joint will affect the cartilage composition which is detected by  $T_{1\rho}$  imaging (112). In 26 subjects with a clinical diagnosis of KL1-3 OA,  $T_{1\rho}$  was found to be significantly higher in medial tibial central cartilage than lateral tibial central cartilage in varus group, suggesting association between knee alignment, therefore different loading to different compartments, and  $T_{1\rho}$  values of femorotibial cartilage in patients with clinical OA (113).

Using a MR-compatible loading device, significant

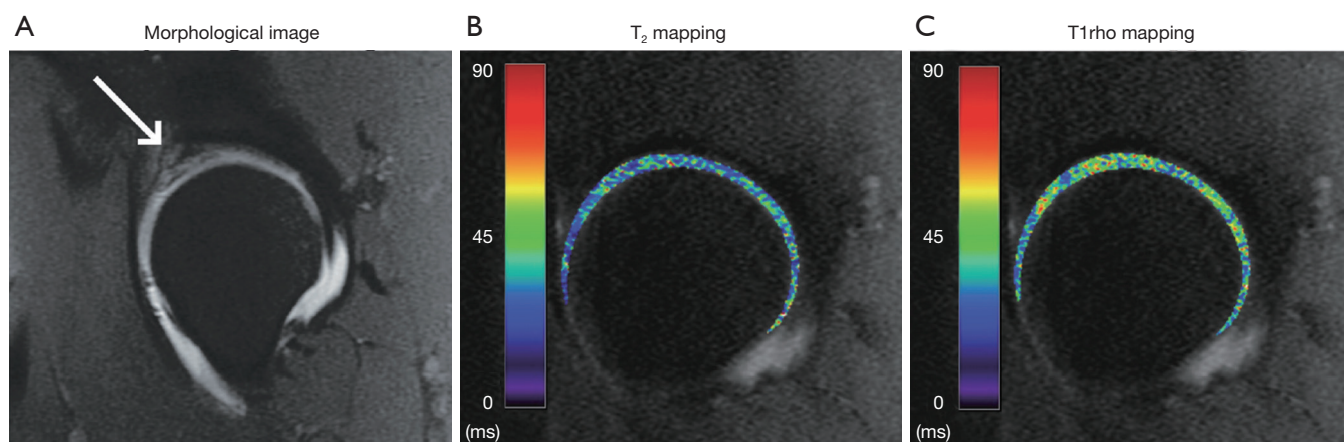


**Figure 11** Quantitative MRI of hip impingement. Sagittal  $T_1$ -weighted image (A) of a patient with mixed impingement demonstrates swelling and increased signal in the anterior-superior labrum, suggesting a tear.  $T_2$  (B) and  $T_{1\rho}$  (C) maps of the same patient demonstrate applications of quantitative imaging to the hip [Reprinted with permission (56)].

decreases of  $T_{1\rho}$  and  $T_2$  were observed with simulated static loading (50% body weight) (114-116). The decreases of relaxation times were probably due to loss of water content and alteration to the matrix structure under acute loading. In 137 subjects with and without knee OA, reductions of  $T_{1\rho}$  and  $T_2$  were larger for subjects with OA (range, 13–19% change) when compared to healthy controls (range, 3–13% change) (116), suggesting loaded  $T_{1\rho}$  and  $T_2$  values can be a sensitive marker for the impaired biomechanical properties of OA cartilage.

In summary,  $T_{1\rho}$  imaging in cartilage can provide valuable information related with biochemical changes in cartilage matrix. In particular, compared to more established  $T_2$  relaxation time,  $T_{1\rho}$  provides more sensitive detection of PG loss at early stages of cartilage degeneration. Similar as  $T_2$  quantification,  $T_{1\rho}$  quantification requires no contrast agent inject and no special hardware, therefore has the great promise to be used in multicenter clinical trials and be translated into clinical practice. Technique challenges of  $T_{1\rho}$  quantification include high energy deposited to tissue (high SAR) and relatively long acquisition time. Advanced acceleration techniques have shown great promise to reduce the acquisition time without sacrifice quantification accuracy (117-119). Advanced image processing tools including robust cartilage segmentation are also critical for accurate  $T_{1\rho}$  quantification. Recent efforts include automatic atlas-based cartilage segmentation and voxel-based relaxometry (VBR) analysis (120,121). In addition to the knee joint,  $T_{1\rho}$  imaging has been applied to other joints such as hip (Figure 11, 122-126).

#### *Applications of $T_{1\rho}$ MR imaging in intervertebral disc*

Musculoskeletal conditions are the most common cause of severe long term pain and physical disability, and they affect hundreds of millions of people around the world. Currently, the global population is experiencing a shift in its age structure due to decreasing fertility rates and increasing longevity. As a result, clinicians worldwide will be required to manage an increasing number of spinal disorders specific to the elderly and the aging of the spine. Spine degeneration and associated clinical symptomatology is a major socioeconomic burden (127-129). Degenerative disc disease of the intervertebral disc is the most common cause of back pain associated disability in adults across the world. Early signs of disc degeneration are manifested by biochemical changes, including a loss of PGs, a loss of osmotic pressure and hydration. In the later stages of disc degeneration, morphological changes occur, including a loss of disc height, disc herniation, annular tears and radial bulging. Disc degeneration can be a combination of a physical aging process and as well as pathological process. In an analysis of published data of 600 autopsy specimens of young and middle-aged subjects younger than 50 years, intervertebral disc degeneration was observed in men in the 2<sup>nd</sup> decade of life, occurring at an earlier age than in women; the severity of aged matched disk degeneration was also being generally greater in men (130). In a later independent histologic study, Łebkowski *et al.* (131) investigated 308 lumbar intervertebral disks at autopsy from 57 women (mean age, 41.8 years) and 79 men (mean age, 42.1 years).

Disk degeneration became first readily apparent during the 2<sup>nd</sup> decade of life, though it was observed to occur in men almost a decade earlier than in women. However, after menopause women show accelerated lumbar disc degeneration compared with men (132,133).

To explore more sensitive imaging biomarkers for disc degeneration, Johannessen *et al.* firstly published  $T_{1\rho}$  imaging of disc *ex vivo* in 2006 (134). Shortly later Blumenkrantz *et al.* published *in vivo* feasibility results (135).  $T_{1\rho}$  imaging allows for spatial measurements on a continuous rather than an integer-based grading, minimizes the potential for observer bias. Although there still exist other technical challenges for  $T_{1\rho}$  imaging such as high SAR (especially at ultrahigh magnetic field strength) and relatively long acquisition time,  $T_{1\rho}$  imaging has the advantages of no contrast agent administration, no RF hardware modification, and the ability to be implemented on any standard clinical scanners. In one recent study of lumbar MRI at 3T (49), It was found for nucleus pulposus (NP),  $T_{1\rho}$  and  $T_2$  decreases quadratically with disc degeneration grades and have no significant trend difference (Figure 12). For annulus fibrosus (AF),  $T_{1\rho}$  decreases linearly as the disc degenerated and has a slope of -3.02 and -4.56 for eight- and five-level gradings respectively; while the slopes for  $T_2$  values are -1.43 and -1.84 respectively, being significantly flatter than those of  $T_{1\rho}$  ( $P < 0.001$ , Figure 2). Therefore  $T_{1\rho}$  is a more sensitive biomarker for early disc AF degeneration. It is also noted in this study that, for both NP and AF, discs of grade 5/8 to 8/8 degenerations had similar  $T_{1\rho}$  and  $T_2$  relaxation times without significant statistical difference. This means when the disc degenerated to a certain extent,  $T_{1\rho}$  and  $T_2$  relaxation time will become insensitive. Therefore, for severe degeneration and disc space narrowing, the 5- or 8-level grading system will remain to be used (136,137). In one study involving 52 subject and at 3T, it was shown an age related reduction of  $T_{1\rho}$  and  $T_2$  magnetic resonance relaxation times both in the NP and the annulus fibrosus of lumbar intervertebral disc. However, the relative performances of  $T_{1\rho}$  vs.  $T_2$  were broadly similar. Actually,  $T_2$  slightly out-performed  $T_{1\rho}$  in NP region, but  $T_{1\rho}$  slightly out-performed  $T_2$  in annulus fibrosus region (Figure 13) (138). In one recent study,  $T_{1\rho}$  value was shown to be significantly lower in asymptomatic young male weightlifters compared with a sedentary control group matched for age and sex (139).

Chronic low back pain is a physical symptom with multiple possible causes; defining the specific source of the pain remains a challenge. In degenerated discs, two

mechanisms of pain have been proposed, i.e., the “chemically sensitized” and “mechanically sensitized” disc. In the former, degenerating discs can undergo an inflammatory process that involves cytokines, such as interleukins and TNF $\alpha$  as well as specific nociceptive mediators such as prostaglandins and NO. In the latter, degenerated discs are no longer intact. Endplate and annular fissures develop that may bring neovascularity and new nerve growth with unmyelinated nerve endings having nociceptive morphologies and neurotransmitters. With compromised mechanical integrity, the transport of nociceptive mediators to its innervated periphery and adjacent structures in degenerated discs would be easier than in healthy discs, where the transport of solutes, especially larger solutes, is limited. Thus, the physician’s inability to identify a patient’s underlying pathology hinders his choice of treatment. However, MRI does not always show sufficient specificity to identify a degenerated disc as the actual source of the pain. The only tool currently available for direct evaluation of disc pain is provocative discography. Due to its invasive nature, there is no agreement on whether it may still be considered a gold standard or even a reliable procedure. A reliable diagnostic tool that could help a clinician to determine if a disc is the source of the pain in patients with chronic lower back pain is still not available (140). MRI findings of disc protrusion, nerve root displacement or compression, disc degeneration, and high intensity zone are all associated with lower back pain, but individually, none of these abnormalities provides a strong indication that lower back pain is attributable to underlying pathology. This limits their value in refining epidemiological case definitions for low back pain (141). Additionally, It has been suggested that researchers should not focus on extending their capacity to find “mildly degenerated”, asymptomatic discs for possible early intervention.

Recently Ogon *et al.* (142) reported that disc’s  $T_2$  relaxation time tended to be lower in the chronic low back pain group than in the control group, and these values were significantly different within the posterior AF. The results indicated a correlation between posterior annulus fibrosus degeneration and chronic low back pain. Ogon *et al.* proposed that chronic low back pain did not show correlations with  $T_2$  values in the anterior annulus fibrosus or NP, but did in the posterior annulus fibrosus, because of low sensitivity against noxious stimuli in the front part of the disc. We expect further studies with  $T_{1\rho}$  based technique may be valuable as  $T_{1\rho}$  is known to be more sensitive for annulus fibrosus than  $T_2$ .

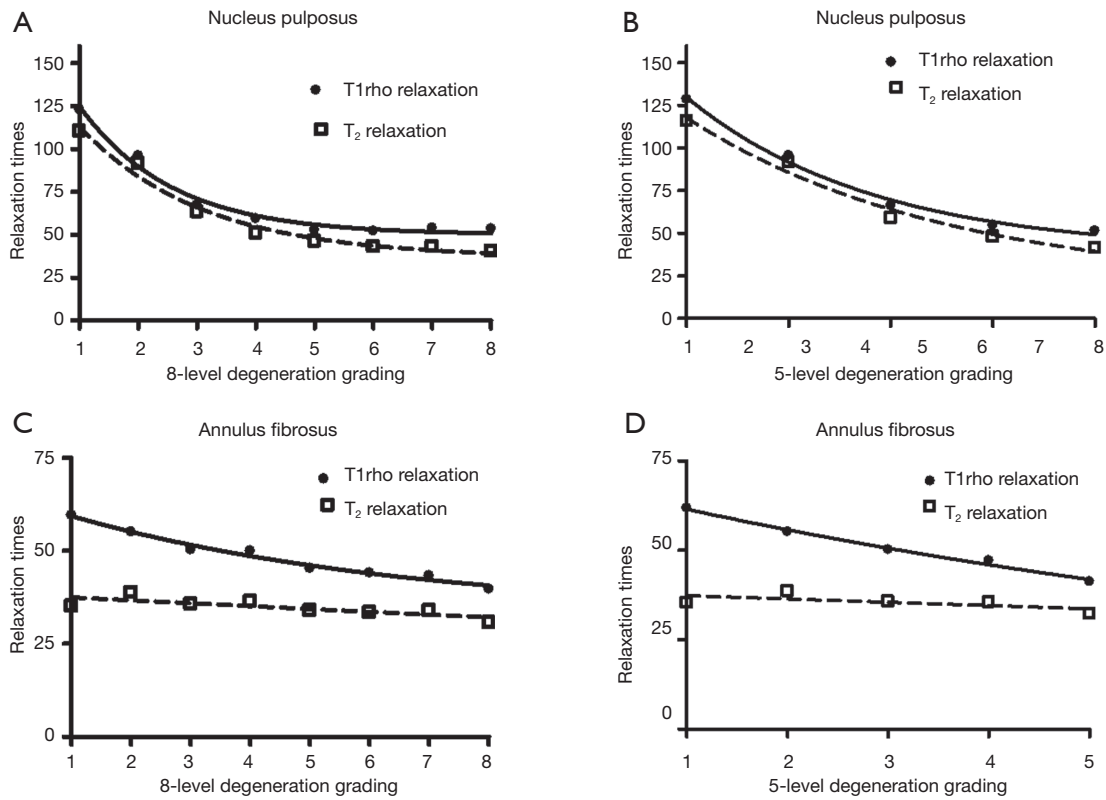


**Figure 12** Thirty-eight subjects (mean age: 48 years; range, 23–71 years) scanned at 3T scanner. For nucleus pulposus (NP),  $T_{1\rho}$  and  $T_2$  values decreased following disc degeneration and had the similar trend ( $P=0.67$ ). For annulus fibrosus,  $T_{1\rho}$  values decreased as disc degenerated and had a slope of  $-2.80$  and  $-4.33$  for 8- and 5-level gradings respectively; while the slopes for  $T_2$  values were  $-1.18$  and  $-1.53$  respectively, being significantly flatter ( $P=0.002$ ) as compared to those of  $T_{1\rho}$ .

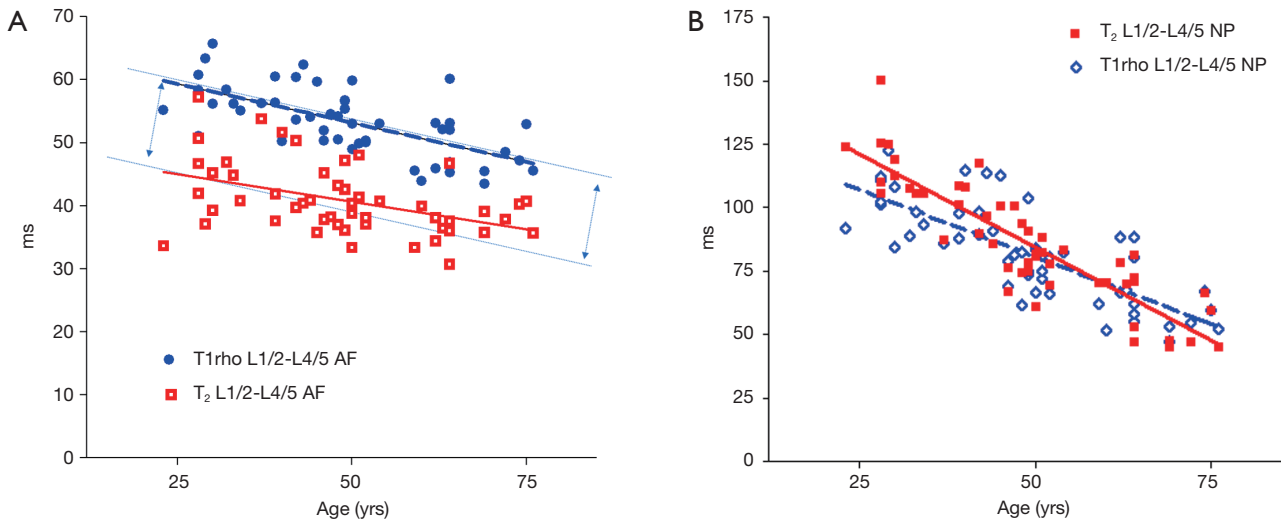


**Figure 13** Aging related reduction of disc relaxation time. (A) Aging related reduction of  $T_{1\rho}$  vs.  $T_2$  of the annulus fibrosus of L1/2-L4/5 discs ( $n=52$  subjects). The slope of  $T_{1\rho}$  is slightly steeper than that of  $T_2$  ( $P=0.31$ ); (B) aging related reduction of  $T_{1\rho}$  vs.  $T_2$  of the nucleus pulposus (NP) of L1/2-L4/5 discs. The slope of  $T_2$  is slightly steeper than that of  $T_{1\rho}$  ( $P=0.085$ ) [Reprinted with permission (138)]. AF, annulus fibrosus.

Therefore, the clinical value and relevance of imaging biomarkers for early cartilage change remain to be further explored (143). The influencing factors for calculating  $T_{1\rho}$  value include individual subject variation, regions of interest (ROIs) measured, water content, spin-lock power, pulse sequence parameters, and protocol settings, etc. Despite the promising results in evaluating small cohorts, the value of individual  $T_{1\rho}$  measurement in a clinical setting requires validation with reference standard, and larger prospective multicenter trials. Salzmann *et al.* evaluate clinical outcomes and the quality of repair tissue after autologous chondrocyte implantation using qualitative MR  $T_2$ -weighted relaxation times. It was found there was only weak correlation of quantitative imaging data and clinical function (144). A critical lack of conclusive evidence still remains to determine whether MRI is reliable in predicting clinical outcomes after cartilage repair and, furthermore, which parameters are most important in determining these outcomes (145,146).

Currently, what is the most efficient approach to obtain  $T_{1\rho}$  imaging of the spine remains to be established. Till now most the published paper obtained only single sagittal plane as  $T_{1\rho}$  imaging is a time consuming technique. Development for speeding-up data acquisition as well as overcoming  $B_0/B_1$  inhomogeneity is continuing. Imperfect flip angle of tip-down/tip-up/refocus pulse due to inhomogeneous  $B_1$  field will complicate the orientation of the net magnetization. The deviation of the effective spin-lock field from the nominal spin-lock field due to inhomogeneous  $B_0$  further complicates the magnetization evolution and leads to signal null (banding artifact) and/or signal contamination from  $T_{2\rho}$  relaxation. Improvement of  $T_{1\rho}$  quantification can be realized either by reducing artifacts from  $T_{1\rho}$ -weighted images and then following the mono-exponential relaxation model for fitting (9), or by fitting the signal intensity of  $T_{1\rho}$ -weighted images even with artifacts to a more complicated magnetization model which is able to quantify  $T_{1\rho}$  and  $T_{2\rho}$  relaxation even in the presence of field imperfections, as demonstrated in the literature (147). The former one works at an image acquisition stage; the latter one works at an image post-processing stage. Wang *et al.* and Yuan *et al.* suggested the feasibility of limited number spin-lock time ( $=3$ ) (148). Zhu *et al.* proposed PANDA- $T_{1\rho}$  approach to reconstruct the  $T_{1\rho}$ -weighted images from under-sampled k-space data and accelerate the acquisition of  $T_{1\rho}$  imaging by a factor of 2–4 (117). Johnson *et al.* proposed precision-guided sampling schedules for efficient  $T_{1\rho}$  mapping (149). The optimal signal of spine tissue already remains to be

further tested (150). For example, Yuan *et al.* showed bi-exponential  $T(1\rho)$  relaxation was observed in muscles with a longer relaxation component of ~37–~41 ms (a fraction of ~80–~88%) and a shorter  $T(1\rho)$  relaxation component of ~9–~11 ms (~12–20%) (151).

Currently there are a number of issues for translational research of novel MR techniques for intervertebral disc evaluation:

- (I) To evaluate one novel MR technique (a new biomarker) against another existing imperfect biomarker, such as the 5-level disc degeneration grading system is not a perfect approach, instead focus should be on evaluating a MR technique against clinical outcomes (152,153). The clinical relevance of disc degeneration grading, i.e. the disc degeneration grading seen on  $T_2$  weighted MRI, remain unknown; instead only disc space narrowing is known to be likely related to lower back pain (154). One study by Blumenkrantz *et al.* (155) that included 16 patients, found a significant correlation between  $T_{1\rho}$  data and clinical symptoms. The relevance of these findings is limited by the small size of the group tested;
- (II) 5-level (and 8 level) disc degeneration grading system are mainly based on  $T_2$  relaxivity, therefore particularly evaluate  $T_2/T_2^*$  measurement against disc degeneration grading are not very meaningful. There are a number of quantitative measures for AF and NP, such as the signal ratio of disc components vs. cerebral spinal fluid (CSF),  $T_2/T_2^*$ ,  $T_{1\rho}$ , CEST (156). The clear advantage of  $T_{1\rho}$  as compared with other measurement needs to be explored and validated, particularly considering  $T_2$  weight anatomical image offer superior spatial resolution and signal-to-noise ratio. The measurement reproducibility for  $T_{1\rho}$  remains to be better established, as well as the influence of susceptibility effect on measurement precision in the targeted regions;
- (III) The best segmentation method for anterior AF, NP, and posterior NP remains to be further explored (157). Actually based on  $T_2$  weighted image, it is very difficult to accurately and comprehensively segment these three components (158). This will be especially problematic in severely degenerated discs. To authors' knowledge, data till now showed  $T_{1\rho}$  map and CEST could not separate inner AF and NP

either. One recent study seemed to show posterior AF degeneration is related to chronic low back pain, but not anterior AF, NP (142), therefore evaluation of posterior AF may be more important. Disc  $T_{1\rho}$  imaging in axial plane may provide more information than sagittal plane. *Ex vivo* study of  $T_{1\rho}$  imaging in axial plane has been reported by Mulligan *et al.* (159);

- (IV) Till now, most studies are cross-sectional, and small in subject number. Few longitudinal studies are available. High quality studies involve clinical endpoints and longitudinal follow-ups will be valuable. Regarding whether the novel MR technique can positively influence clinical management, there are many further questions: (I) can the disc changes detected by novel MR technique amenable to some medical or surgical interventions; (II) what MRI detected disc changes are physiological aging? (III) will some disc changes detected by highly sensitive novel MR technique leading to over-treatment, as they may recover or repair by the physiological mechanism. Some lesions can be learnt from the cancer screen studies. More than two decades of cancer screen for breast cancer and prostate cancer showed that high sensitivity based method leads to many false positive results and over treatment (160-163). Early detection of diseases has intuitive assumption any deviations—subtle or apparent—from a clearly demarcated “normal” were to be corrected, given the underlying hypothesis that diseases develop along progressive linear paths of increasing abnormalities. However, now it is understood that screening of non-symptomatic subjects may even do more harm (160,162).

### Challenges and forward looking

A number of RF pulse cluster for  $T_{1\rho}$  prep have been proposed to improve the robustness of  $T_{1\rho}$  prep against system imperfection. Comprehensive studies to compare these methods can help users to choose the right approach for specific study. Despite the significant improvement of robustness of  $T_{1\rho}$  prep at the presence of  $B_1$  RF and  $B_0$  field inhomogeneity, residual artifacts can still be observed at certain cases with these methods. Further work is still needed to improve the effectiveness of  $T_{1\rho}$  prep RF pulses in terms of compensation of  $B_1$  RF and  $B_0$  field inhomogeneity.

Various data acquisition methods have been reported for data acquisition in  $T_{1\rho}$  imaging, with a few of them for 3D quantitative  $T_{1\rho}$  imaging (12-14,16). Different data acquisition may result in different  $T_{1\rho}$  value. A systematic study to compare these methods and understand the pros and cons of each of them can be very beneficial to setup a norm for  $T_{1\rho}$  imaging in the field.

For routine clinical use, the establishment of the reproducibility of  $T_{1\rho}$  measurement is essential. A few reproducibility studies have been carried out recently (72,164). It will be very beneficial to have comprehensive reproducibility studies performed with different time span, at different system, at systems from different vendors, and at different sites.

The change of  $T_{1\rho}$  value between the healthy state and diseased state can be small. However, the sources which cause errors of  $T_{1\rho}$  quantification are multiple, including  $B_1$  RF inhomogeneity and  $B_0$  field inhomogeneity and data acquisition. With the demand of fast data acquisition and high spatial resolution, it inevitably results in loss of SNR, which increases the risks of quantification error. Without providing confidence level of measured  $T_{1\rho}$  value, it is difficult for users to make clinical diagnosis based on measured  $T_{1\rho}$  map. It is one of the major challenges to establish such confidence level in quantitative  $T_{1\rho}$  imaging.

A major application of  $T_{1\rho}$  is in cartilage. However, the presence of magic angle effect can confound its use. Magic angle effect may be mitigated by increasing spin lock frequency (165). However, the maximum spin lock frequency available in a clinical scanner is limited by the power of RF amplifier and SAR. Further investigation may be needed to address magic angle effect. In cartilage, there usually exist three groups of tissues with ultra-shot, intermediate, and long  $T_{1\rho}$  relaxation, respectively. Typically measured  $T_{1\rho}$  value is the average of the intermediate and long  $T_{1\rho}$  value. Multi-component analysis may help improve the diagnostic value of  $T_{1\rho}$ , but at cost of scan time. Further technical work to improve data acquisition speed for multi-component analysis is needed.

### Acknowledgements

The authors thank Mr. Wang Junqing for the help during manuscript preparation.

*Funding:* This study was partially supported by grants from the Research Grants Council of the Hong Kong SAR (Project No. 476313 and Project No. SEG\_CUHK02).

## Footnote

*Conflicts of Interest:* The authors have no conflicts of interest to declare.

## References

1. Redfield AG. Nuclear magnetic resonance saturation and rotary saturation in solids. *Phys Rev* 1955;98:1787.
2. Markkola A. Spin lock and Magnetization transfer imaging of head and neck tumors. Academic Dissertation. Faculty of Medicine of the University of Helsinki, Helsinki 2003. Available online: <https://helda.helsinki.fi/bitstream/handle/10138/22600/spinlock.pdf?sequence=2>
3. Sepponen RE, Pohjonen JA, Sipponen JT, Tantt JI. A method for T1 rho imaging. *J Comput Assist Tomogr* 1985;9:1007-11.
4. Markkola AT, Aronen HJ, Paavonen T, Hopsu E, Sipilä LM, Tantt JI, Sepponen RE. Spin lock and magnetization transfer imaging of head and neck tumors. *Radiology* 1996;200:369-75.
5. Hulvershorn J, Borthakur A, Bloy L, Gualtieri EE, Reddy R, Leigh JS, Elliott MA. T1rho contrast in functional magnetic resonance imaging. *Magn Reson Med* 2005;54:1155-62.
6. Charagundla SR, Borthakur A, Leigh JS, Reddy R. Artifacts in T(1rho)-weighted imaging: correction with a self-compensating spin-locking pulse. *J Magn Reson* 2003;162:113-21.
7. Yuan J, Li Y, Zhao F, Chan Q, Ahuja AT, Wang YX. Quantification of T(1ρ) relaxation by using rotary echo spin-lock pulses in the presence of B(0) inhomogeneity. *Phys Med Biol* 2012;57:5003-16.
8. Witschey WR 2nd, Borthakur A, Elliott MA, Mellon E, Niyogi S, Wallman DJ, Wang C, Reddy R. Artifacts in T1 rho-weighted imaging: compensation for B(1) and B(0) field imperfections. *J Magn Reson* 2007;186:75-85.
9. Li Y, Zhao F, Wang YX, Ahuja AT, Yuan J. Study of magnetization evolution by using composite spin-lock pulses for T1ρ imaging. *Conf Proc IEEE Eng Med Biol Soc* 2012;2012:408-11.
10. Li X, Han ET, Ma CB, Link TM, Newitt DC, Majumdar S. In vivo 3T spiral imaging based multi-slice T(1rho) mapping of knee cartilage in osteoarthritis. *Magn Reson Med* 2005;54:929-36.
11. Chen W, Takahashi A, Han E. Quantitative T(1) (ρ) imaging using phase cycling for B0 and B1 field inhomogeneity compensation. *Magn Reson Imaging* 2011;29:608-19.
12. Borthakur A, Wheaton A, Charagundla SR, Shapiro EM, Regatte RR, Akella SV, Kneeland JB, Reddy R. Three-dimensional T1rho-weighted MRI at 1.5 Tesla. *J Magn Reson Imaging* 2003;17:730-6.
13. Li X, Han ET, Busse RF, Majumdar S. In vivo T(1rho) mapping in cartilage using 3D magnetization-prepared angle-modulated partitioned k-space spoiled gradient echo snapshots (3D MAPSS). *Magn Reson Med* 2008;59:298-307.
14. Chen WT, Han ET. 3D quantitative imaging of T1rho and T2. *Proc Annual Meeting ISMRM* 2011;231.
15. Duvvuri U, Charagundla SR, Kudchodkar SB, Kaufman JH, Kneeland JB, Rizi R, Leigh JS, Reddy R. Human knee: in vivo T1(rho)-weighted MR imaging at 1.5 T-- preliminary experience. *Radiology* 2001;220:822-6.
16. Witschey WR, Borthakur A, Elliott MA, Fenty M, Sochor MA, Wang C, Reddy R. T1rho-prepared balanced gradient echo for rapid 3D T1rho MRI. *J Magn Reson Imaging* 2008;28:744-54.
17. Collins CM, Li S, Smith MB. SAR and B1 field distributions in a heterogeneous human head model within a birdcage coil. Specific energy absorption rate. *Magn Reson Med* 1998;40:847-56.
18. Yuan J, Zhao F, Griffith JF, Chan Q, Wang YX. Optimized efficient liver T(1ρ) mapping using limited spin lock times. *Phys Med Biol* 2012;57:1631-40.
19. Griswold MA, Jakob PM, Heidemann RM, Nittka M, Jellus V, Wang J, Kiefer B, Haase A. Generalized autocalibrating partially parallel acquisitions (GRAPPA). *Magn Reson Med* 2002;47:1202-10.
20. Pruessmann KP, Weiger M, Scheidegger MB, Boesiger P. SENSE: sensitivity encoding for fast MRI. *Magn Reson Med* 1999;42:952-62.
21. Sodickson DK, Manning WJ. Simultaneous acquisition of spatial harmonics (SMASH): fast imaging with radiofrequency coil arrays. *Magn Reson Med* 1997;38:591-603.
22. Liang D, DiBella EV, Chen RR, Ying L. k-t ISD: dynamic cardiac MR imaging using compressed sensing with iterative support detection. *Magn Reson Med* 2012;68:41-53.
23. Lustig M, Donoho D, Pauly JM. Sparse MRI: The application of compressed sensing for rapid MR imaging. *Magn Reson Med* 2007;58:1182-95.
24. Yuan J, Liang D, Zhao F, Li Y, Wang YX, Ying L. k-t ISD compressed sensing reconstruction for T1ρ mapping: A study in rat brains at 3T. *Proc Intl Soc Mag Reson Med*

- 2012:4197.
25. Wheaton AJ, Borthakur A, Corbo M, Charagundla SR, Reddy R. Method for reduced SAR T<sub>1ρ</sub>-weighted MRI. *Magn Reson Med* 2004;51:1096-102.
  26. Yuan J, Zhao TC, Tang Y, Panych LP. Reduced field-of-view single-shot fast spin echo imaging using two-dimensional spatially selective radiofrequency pulses. *J Magn Reson Imaging* 2010;32:242-8.
  27. Rieseberg S, Frahm J, Finsterbusch J. Two-dimensional spatially-selective RF excitation pulses in echo-planar imaging. *Magn Reson Med* 2002;47:1186-93.
  28. Zhu Y. Parallel excitation with an array of transmit coils. *Magn Reson Med* 2004;51:775-84.
  29. Jokivarsi KT, Niskanen JP, Michaeli S, Gröhn HI, Garwood M, Kauppinen RA, Gröhn OH. Quantitative assessment of water pools by T<sub>1ρ</sub> and T<sub>2ρ</sub> MRI in acute cerebral ischemia of the rat. *J Cereb Blood Flow Metab* 2009;29:206-16.
  30. Mäkelä HI, Kettunen MI, Gröhn OH, Kauppinen RA. Quantitative T<sub>1ρ</sub> and magnetization transfer magnetic resonance imaging of acute cerebral ischemia in the rat. *J Cereb Blood Flow Metab* 2002;22:547-58.
  31. Gröhn OH, Lukkarinen JA, Silvennoinen MJ, Pitkänen A, van Zijl PC, Kauppinen RA. Quantitative magnetic resonance imaging assessment of cerebral ischemia in rat using on-resonance T<sub>1</sub> in the rotating frame. *Magn Reson Med* 1999;42:268-76.
  32. Gröhn OHJ, Kettunen MI, Mäkelä HI, Penttonen M, Pitkänen A, Lukkarinen JA, Kauppinen RA. Early detection of irreversible cerebral ischemia in the rat using dispersion of the magnetic resonance imaging relaxation time, T<sub>1ρ</sub>. *J Cereb Blood Flow Metab* 2000;20:1457-66.
  33. Nestrasil I, Michaeli S, Liimatainen T, Rydeen CE, Kotz CM, Nixon JP, Hanson T, Tuite PJ. T<sub>1ρ</sub> and T<sub>2ρ</sub> MRI in the evaluation of Parkinson's disease. *J Neurol* 2010;257:964-8.
  34. Haris M, Singh A, Cai K, McArdle E, Fenty M, Davatzikos C, Trojanowski JQ, Melhem ER, Clark CM, Borthakur A. T<sub>1ρ</sub> MRI in Alzheimer's disease: detection of pathological changes in medial temporal lobe. *J Neuroimaging* 2011;21:e86-90.
  35. Haris M, Singh A, Cai K, Davatzikos C, Trojanowski JQ, Melhem ER, Clark CM, Borthakur A. T<sub>1ρ</sub> (T<sub>1ρ</sub>) MR imaging in Alzheimer's disease and Parkinson's disease with and without dementia. *J Neurol* 2011;258:380-5.
  36. Haris M, McArdle E, Fenty M, Singh A, Davatzikos C, Trojanowski JQ, Melhem ER, Clark CM, Borthakur A. Early marker for Alzheimer's disease: hippocampus T<sub>1ρ</sub> (T<sub>1ρ</sub>) estimation. *J Magn Reson Imaging* 2009;29:1008-12.
  37. Borthakur A, Sochor M, Davatzikos C, Trojanowski JQ, Clark CM. T<sub>1ρ</sub> MRI of Alzheimer's disease. *Neuroimage* 2008;41:1199-205.
  38. Zhao F, Yuan J, Lu G, Zhang LH, Chen ZY, Wáng YJ. T<sub>1ρ</sub> relaxation time in brain regions increases with ageing: an experimental MRI observation in rats. *Br J Radiol* 2016;89:20140704.
  39. Han Y, Liimatainen T, Gorman RC, Witschey WR. Assessing Myocardial Disease Using T<sub>1ρ</sub> MRI. *Curr Cardiovasc Imaging Rep* 2014;7:9248.
  40. Witschey WR, Zsido GA, Koomalsingh K, Kondo N, Minakawa M, Shuto T, McGarvey JR, Levack MM, Contijoch F, Pilla JJ, Gorman JH 3rd, Gorman RC. In vivo chronic myocardial infarction characterization by spin locked cardiovascular magnetic resonance. *J Cardiovasc Magn Reson* 2012;14:37.
  41. Singh A, Reddy D, Haris M, Cai K, Reddy KR, Hariharan H, Reddy R. T<sub>1ρ</sub> MRI of healthy and fibrotic human livers at 1.5 T. *J Transl Med* 2015;13:292.
  42. Wang YX, Yuan J. Evaluation of liver fibrosis with T<sub>1ρ</sub> MR imaging. *Quant Imaging Med Surg* 2014;4:152-5.
  43. Allkemper T, Sagmeister F, Cicinnati V, Beckebaum S, Kooijman H, Kanthak C, Stehling C, Heindel W. Evaluation of fibrotic liver disease with whole-liver T<sub>1ρ</sub> MR imaging: a feasibility study at 1.5 T. *Radiology* 2014;271:408-15.
  44. Zhao F, Wang YX, Yuan J, Deng M, Wong HL, Chu ES, Go MY, Teng GJ, Ahuja AT, Yu J. MR T<sub>1ρ</sub> as an imaging biomarker for monitoring liver injury progression and regression: an experimental study in rats with carbon tetrachloride intoxication. *Eur Radiol* 2012;22:1709-16.
  45. Wang YX, Yuan J, Chu ES, Go MY, Huang H, Ahuja AT, Sung JJ, Yu J. T<sub>1ρ</sub> MR imaging is sensitive to evaluate liver fibrosis: an experimental study in a rat biliary duct ligation model. *Radiology* 2011;259:712-9.
  46. Virta A, Komu M, Lundbom N, Kormanen M. T<sub>1ρ</sub> MR imaging characteristics of human anterior tibial and gastrocnemius muscles. *Acad Radiol* 1998;5:104-10.
  47. Lamminen AE, Tanttú JI, Sepponen RE, Pihko H, Korhola OA. T<sub>1ρ</sub> dispersion imaging of diseased muscle tissue. *Br J Radiol* 1993;66:783-7.
  48. Sierra A, Michaeli S, Niskanen JP, Valonen PK, Gröhn HI, Ylä-Herttua S, Garwood M, Gröhn OH. Water spin dynamics during apoptotic cell death in glioma gene therapy probed by T<sub>1ρ</sub> and T<sub>2ρ</sub>. *Magn Reson Med* 2008;59:1311-9.

49. Wang YX, Zhao F, Griffith JF, Mok GS, Leung JC, Ahuja AT, Yuan J. T1rho and T2 relaxation times for lumbar disc degeneration: an in vivo comparative study at 3.0-Tesla MRI. *Eur Radiol* 2013;23:228-34.
50. Wang L, Regatte RR. T1ρ MRI of human musculoskeletal system. *J Magn Reson Imaging* 2015;41:586-600.
51. Murphy L, Schwartz TA, Helmick CG, Renner JB, Tudor G, Koch G, Dragomir A, Kalsbeek WD, Luta G, Jordan JM. Lifetime risk of symptomatic knee osteoarthritis. *Arthritis Rheum* 2008;59:1207-13.
52. Helmick CG, Felson DT, Lawrence RC, Gabriel S, Hirsch R, Kwoh CK, Liang MH, Kremers HM, Mayes MD, Merkel PA, Pillemer SR, Reveille JD, Stone JH; National Arthritis Data Workgroup. Estimates of the prevalence of arthritis and other rheumatic conditions in the United States. Part I. *Arthritis Rheum* 2008;58:15-25.
53. Murray CJ, Vos T, Lozano R, Naghavi M, Flaxman AD, Michaud C, Ezzati M, Shibuya K, Salomon JA, Abdalla S, Aboyans V, Abraham J, Ackerman I, Aggarwal R, Ahn SY, Ali MK, Alvarado M, Anderson HR, Anderson LM, Andrews KG, Atkinson C, Baddour LM, Bahalim AN, Barker-Collo S, Barrero LH, Bartels DH, Basáñez MG, Baxter A, Bell ML, Benjamin EJ, Bennett D, Bernabé E, Bhalla K, Bhandari B, Bikbov B, Bin Abdulhak A, Birbeck G, Black JA, Blencowe H, Blore JD, Blyth F, Bolliger I, Bonaventure A, Boufous S, Bourne R, Boussinesq M, Braithwaite T, Brayne C, Bridgett L, Brooker S, Brooks P, Brugha TS, Bryan-Hancock C, Bucello C, Buchbinder R, Buckle G, Budke CM, Burch M, Burney P, Burstein R, Calabria B, Campbell B, Canter CE, Carabin H, Carapetis J, Carmona L, Cella C, Charlson F, Chen H, Cheng AT, Chou D, Chugh SS, Coffeng LE, Colan SD, Colquhoun S, Colson KE, Condon J, Connor MD, Cooper LT, Corriere M, Cortinovis M, de Vaccaro KC, Couser W, Cowie BC, Criqui MH, Cross M, Dabhadkar KC, Dahiya M, Dahodwala N, Damsere-Derry J, Danaei G, Davis A, De Leo D, Degenhardt L, Dellavalle R, Delossantos A, Denenberg J, Derrett S, Des Jarlais DC, Dharmaratne SD, Dherani M, Diaz-Torne C, Dolk H, Dorsey ER, Driscoll T, Duber H, Ebel B, Edmond K, Elbaz A, Ali SE, Erskine H, Erwin PJ, Espindola P, Ewoigbokhan SE, Farzadfar F, Feigin V, Felson DT, Ferrari A, Ferri CP, Fèvre EM, Finucane MM, Flaxman S, Flood L, Foreman K, Forouzanfar MH, Fowkes FG, Fransen M, Freeman MK, Gabbe BJ, Gabriel SE, Gakidou E, Ganatra HA, Garcia B, Gaspari F, Gillum RF, Gmel G, Gonzalez-Medina D, Gosselin R, Grainger R, Grant B, Groeger J, Guillemin F, Gunnell D, Gupta R, Haagsma J, Hagan H, Halasa YA, Hall W, Haring D, Haro JM, Harrison JE, Havmoeller R, Hay RJ, Higashi H, Hill C, Hoen B, Hoffman H, Hotez PJ, Hoy D, Huang JJ, Ibeanusi SE, Jacobsen KH, James SL, Jarvis D, Jasrasaria R, Jayaraman S, Johns N, Jonas JB, Karthikeyan G, Kassebaum N, Kawakami N, Keren A, Khoo JP, King CH, Knowlton LM, Kobusingye O, Koranteng A, Krishnamurthi R, Laden F, Lalloo R, Laslett LL, Lathlean T, Leasher JL, Lee YY, Leigh J, Levinson D, Lim SS, Limb E, Lin JK, Lipnick M, Lipshultz SE, Liu W, Loane M, Ohno SL, Lyons R, Mabweijano J, MacIntyre MF, Malekzadeh R, Mallinger L, Manivannan S, Marcenes W, March L, Margolis DJ, Marks GB, Marks R, Matsumori A, Matzopoulos R, Mayosi BM, McAnulty JH, McDermott MM, McGill N, McGrath J, Medina-Mora ME, Meltzer M, Mensah GA, Merriman TR, Meyer AC, Miglioli V, Miller M, Miller TR, Mitchell PB, Mock C, Mocumbi AO, Moffitt TE, Mokdad AA, Monasta L, Montico M, Moradi-Lakeh M, Moran A, Morawska L, Mori R, Murdoch ME, Mwaniki MK, Naidoo K, Nair MN, Naldi L, Narayan KM, Nelson PK, Nelson RG, Nevitt MC, Newton CR, Nolte S, Norman P, Norman R, O'Donnell M, O'Hanlon S, Olives C, Omer SB, Ortblad K, Osborne R, Ozgediz D, Page A, Pahari B, Pandian JD, Rivero AP, Patten SB, Pearce N, Padilla RP, Perez-Ruiz F, Perico N, Pesudovs K, Phillips D, Phillips MR, Pierce K, Pion S, Polanczyk GV, Polinder S, Pope CA 3rd, Popova S, Porrini E, Pourmalek F, Prince M, Pullan RL, Ramaiah KD, Ranganathan D, Razavi H, Regan M, Rehm JT, Rein DB, Remuzzi G, Richardson K, Rivara FP, Roberts T, Robinson C, De León FR, Ronfani L, Room R, Rosenfeld LC, Rushton L, Sacco RL, Saha S, Sampson U, Sanchez-Riera L, Sanman E, Schwebel DC, Scott JG, Segui-Gomez M, Shahraz S, Shepard DS, Shin H, Shivakoti R, Singh D, Singh GM, Singh JA, Singleton J, Sleet DA, Sliwa K, Smith E, Smith JL, Stapelberg NJ, Steer A, Steiner T, Stolk WA, Stovner LJ, Sudfeld C, Syed S, Tamburlini G, Tavakkoli M, Taylor HR, Taylor JA, Taylor WJ, Thomas B, Thomson WM, Thurston GD, Tleyjeh IM, Tonelli M, Towbin JA, Truelsen T, Tsilimbaris MK, Ubeda C, Undurraga EA, van der Werf MJ, van Os J, Vavilala MS, Venketasubramanian N, Wang M, Wang W, Watt K, Weatherall DJ, Weinstock MA, Weintraub R, Weisskopf MG, Weissman MM, White RA, Whiteford H, Wiebe N, Wiersma ST, Wilkinson JD, Williams HC, Williams SR, Witt E, Wolfe F, Woolf AD, Wulf S, Yeh PH, Zaidi AK, Zheng ZJ, Zonies D, Lopez AD, AlMazroa MA, Memish ZA. Disability-adjusted life years (DALYs) for 291 diseases and injuries in 21 regions, 1990-2010: a systematic analysis

- for the Global Burden of Disease Study 2010. *Lancet* 2012;380:2197-223.
54. Mankin HJ, Brandt KD. Pathogenesis of arthritis. *Textbook of Rheumatology*. Philadelphia: W.B. Saunders, 1993.
  55. Li X, Majumdar S. Quantitative MRI of articular cartilage and its clinical applications. *J Magn Reson Imaging* 2013;38:991-1008.
  56. Matzat SJ, van Tiel J, Gold GE, Oei EH. Quantitative MRI techniques of cartilage composition. *Quant Imaging Med Surg* 2013;3:162-74.
  57. Link TM, Stahl R, Woertler K. Cartilage imaging: motivation, techniques, current and future significance. *Eur Radiol* 2007;17:1135-46.
  58. Potter HG, Black BR, Chong le R. New techniques in articular cartilage imaging. *Clin Sports Med* 2009;28:77-94.
  59. Akella SV, Regatte RR, Gougoutas AJ, Borthakur A, Shapiro EM, Kneeland JB, Leigh JS, Reddy R. Proteoglycan-induced changes in T1rho-relaxation of articular cartilage at 4T. *Magn Reson Med* 2001;46:419-23.
  60. Regatte RR, Akella SV, Borthakur A, Kneeland JB, Reddy R. Proteoglycan depletion-induced changes in transverse relaxation maps of cartilage: comparison of T2 and T1rho. *Acad Radiol* 2002;9:1388-94.
  61. Akella SV, Regatte RR, Wheaton AJ, Borthakur A, Reddy R. Reduction of residual dipolar interaction in cartilage by spin-lock technique. *Magn Reson Med* 2004;52:1103-9.
  62. Li X, Cheng J, Lin K, Saadat E, Bolbos RI, Jobke B, Ries MD, Horvai A, Link TM, Majumdar S. Quantitative MRI using T1ρ and T2 in human osteoarthritic cartilage specimens: correlation with biochemical measurements and histology. *Magn Reson Imaging* 2011;29:324-34.
  63. Regatte RR, Akella SV, Lonner JH, Kneeland JB, Reddy R. T1rho relaxation mapping in human osteoarthritis (OA) cartilage: comparison of T1rho with T2. *J Magn Reson Imaging* 2006;23:547-53.
  64. Wheaton AJ, Dodge GR, Elliott DM, Nicoll SB, Reddy R. Quantification of cartilage biomechanical and biochemical properties via T1rho magnetic resonance imaging. *Magn Reson Med* 2005;54:1087-93.
  65. Tang SY, Souza RB, Ries M, Hansma PK, Alliston T, Li X. Local tissue properties of human osteoarthritic cartilage correlate with magnetic resonance T(1) rho relaxation times. *J Orthop Res* 2011;29:1312-9.
  66. Rautiainen J, Nissi MJ, Salo EN, Tiitu V, Finnilä MA, Aho OM, Saarakkala S, Lehenkari P, Ellermann J, Nieminen MT. Multiparametric MRI assessment of human articular cartilage degeneration: Correlation with quantitative histology and mechanical properties. *Magn Reson Med* 2014. [Epub ahead of print]. doi: 10.1002/mrm.25401.
  67. Keenan KE, Besier TF, Pauly JM, Smith RL, Delp SL, Beaupre GS, Gold GE. T1ρ Dispersion in Articular Cartilage: Relationship to Material Properties and Macromolecular Content. *Cartilage* 2015;6:113-22.
  68. Mäkelä HI, Gröhn OH, Kettunen MI, Kauppinen RA. Proton exchange as a relaxation mechanism for T1 in the rotating frame in native and immobilized protein solutions. *Biochem Biophys Res Commun* 2001;289:813-8.
  69. Duvvuri U, Goldberg AD, Kranz JK, Hoang L, Reddy R, Wehrli FW, Wand AJ, Englander SW, Leigh JS. Water magnetic relaxation dispersion in biological systems: the contribution of proton exchange and implications for the noninvasive detection of cartilage degradation. *Proc Natl Acad Sci U S A* 2001;98:12479-84.
  70. Kettunen MI, Gröhn OH, Silvennoinen MJ, Penttonen M, Kauppinen RA. Effects of intracellular pH, blood, and tissue oxygen tension on T1rho relaxation in rat brain. *Magn Reson Med* 2002;48:470-7.
  71. Mlynárik V, Szomolányi P, Toffanin R, Vittur F, Trattinig S. Transverse relaxation mechanisms in articular cartilage. *J Magn Reson* 2004;169:300-7.
  72. Li X, Wyatt C, Rivoire J, Han E, Chen W, Schooler J, Liang F, Shet K, Souza R, Majumdar S. Simultaneous acquisition of T1ρ and T2 quantification in knee cartilage: repeatability and diurnal variation. *J Magn Reson Imaging* 2014;39:1287-93.
  73. Mosher TJ, Zhang Z, Reddy R, Boudhar S, Milestone BN, Morrison WB, Kwok CK, Eckstein F, Witschey WR, Borthakur A. Knee articular cartilage damage in osteoarthritis: analysis of MR image biomarker reproducibility in ACRIN-PA 4001 multicenter trial. *Radiology* 2011;258:832-42.
  74. Li X, Podoia V, Kumar D, Rivoire J, Wyatt C, Lansdown D, Amano K, Okazaki N, Savic D, Koff MF, Felmlee J, Williams SL, Majumdar S. Cartilage T1ρ and T2 relaxation times: longitudinal reproducibility and variations using different coils, MR systems and sites. *Osteoarthritis Cartilage* 2015;23:2214-23.
  75. Stahl R, Luke A, Li X, Carballido-Gamio J, Ma CB, Majumdar S, Link TM. T1rho, T2 and focal knee cartilage abnormalities in physically active and sedentary healthy subjects versus early OA patients--a 3.0-Tesla MRI study. *Eur Radiol* 2009;19:132-43.
  76. Kumar D, Souza RB, Subburaj K, MacLeod TD, Singh J, Calixto NE, Nardo L, Link TM, Li X, Lane NE,

- Majumdar S. Are There Sex Differences in Knee Cartilage Composition and Walking Mechanics in Healthy and Osteoarthritis Populations? *Clin Orthop Relat Res* 2015;473:2548-58.
77. Regatte RR, Akella SV, Wheaton AJ, Lech G, Borthakur A, Kneeland JB, Reddy R. 3D-T1rho-relaxation mapping of articular cartilage: in vivo assessment of early degenerative changes in symptomatic osteoarthritic subjects. *Acad Radiol* 2004;11:741-9.
  78. Li X, Benjamin Ma C, Link TM, Castillo DD, Blumenkrantz G, Lozano J, Carballido-Gamio J, Ries M, Majumdar S. In vivo T(1rho) and T(2) mapping of articular cartilage in osteoarthritis of the knee using 3 T MRI. *Osteoarthritis Cartilage* 2007;15:789-97.
  79. Bolbos RI, Zuo J, Banerjee S, Link TM, Ma CB, Li X, Majumdar S. Relationship between trabecular bone structure and articular cartilage morphology and relaxation times in early OA of the knee joint using parallel MRI at 3 T. *Osteoarthritis Cartilage* 2008;16:1150-9.
  80. Wang L, Chang G, Xu J, Vieira RL, Krasnokutsky S, Abramson S, Regatte RR. T1rho MRI of menisci and cartilage in patients with osteoarthritis at 3T. *Eur J Radiol* 2012;81:2329-36.
  81. Thuillier DU, Souza RB, Wu S, Luke A, Li X, Feeley BT. T1ρ imaging demonstrates early changes in the lateral patella in patients with patellofemoral pain and maltracking. *Am J Sports Med* 2013;41:1813-8.
  82. Nishioka H, Hirose J, Okamoto N, Okada T, Oka K, Taniwaki T, Nakamura E, Yamashita Y, Mizuta H. Evaluation of the relationship between T1ρ and T2 values and patella cartilage degeneration in patients of the same age group. *Eur J Radiol* 2015;84:463-8.
  83. Lozano J, Li X, Link TM, Safran M, Majumdar S, Ma CB. Detection of posttraumatic cartilage injury using quantitative T1rho magnetic resonance imaging. A report of two cases with arthroscopic findings. *J Bone Joint Surg Am* 2006;88:1349-52.
  84. Witschey WR, Borthakur A, Fenty M, Kneeland BJ, Lonner JH, McArdle EL, Sochor M, Reddy R. T1rho MRI quantification of arthroscopically confirmed cartilage degeneration. *Magn Reson Med* 2010;63:1376-82.
  85. Nishioka H, Hirose J, Nakamura E, Okamoto N, Karasugi T, Taniwaki T, Okada T, Yamashita Y, Mizuta H. Detecting ICRS grade 1 cartilage lesions in anterior cruciate ligament injury using T1ρ and T2 mapping. *Eur J Radiol* 2013;82:1499-505.
  86. Gupta R, Virayavanich W, Kuo D, Su F, Link T, Ma B, Li X. MR T(1)ρ quantification of cartilage focal lesions in acutely injured knees: correlation with arthroscopic evaluation. *Magn Reson Imaging* 2014;32:1290-6.
  87. Holtzman DJ, Theologis AA, Carballido-Gamio J, Majumdar S, Li X, Benjamin C. T(1ρ) and T(2) quantitative magnetic resonance imaging analysis of cartilage regeneration following microfracture and mosaicplasty cartilage resurfacing procedures. *J Magn Reson Imaging* 2010;32:914-23.
  88. Theologis AA, Schairer WW, Carballido-Gamio J, Majumdar S, Li X, Ma CB. Longitudinal analysis of T1ρ and T2 quantitative MRI of knee cartilage laminar organization following microfracture surgery. *Knee* 2012;19:652-7.
  89. Jungmann PM, Baum T, Bauer JS, Karampinos DC, Erdle B, Link TM, Li X, Trattnig S, Rummeny EJ, Woertler K, Welsch GH. Cartilage repair surgery: outcome evaluation by using noninvasive cartilage biomarkers based on quantitative MRI techniques? *Biomed Res Int* 2014;2014:840170.
  90. Carballido-Gamio J, Link TM, Majumdar S. New techniques for cartilage magnetic resonance imaging relaxation time analysis: texture analysis of flattened cartilage and localized intra- and inter-subject comparisons. *Magn Reson Med* 2008;59:1472-7.
  91. Carballido-Gamio J, Stahl R, Blumenkrantz G, Romero A, Majumdar S, Link TM. Spatial analysis of magnetic resonance T1rho and T2 relaxation times improves classification between subjects with and without osteoarthritis. *Med Phys* 2009;36:4059-67.
  92. Li X, Pai A, Blumenkrantz G, Carballido-Gamio J, Link T, Ma B, Ries M, Majumdar S. Spatial distribution and relationship of T1rho and T2 relaxation times in knee cartilage with osteoarthritis. *Magn Reson Med* 2009;61:1310-8.
  93. Schooler J, Kumar D, Nardo L, McCulloch C, Li X, Link TM, Majumdar S. Longitudinal evaluation of T1ρ and T2 spatial distribution in osteoarthritic and healthy medial knee cartilage. *Osteoarthritis Cartilage* 2014;22:51-62.
  94. Zarins ZA, Bolbos RI, Pialat JB, Link TM, Li X, Souza RB, Majumdar S. Cartilage and meniscus assessment using T1rho and T2 measurements in healthy subjects and patients with osteoarthritis. *Osteoarthritis Cartilage* 2010;18:1408-16.
  95. Takahashi K, Hashimoto S, Nakamura H, Mori A, Sato A, Majima T, Takai S. Medial meniscal posterior root/horn radial tears correlate with cartilage degeneration detected by T1ρ relaxation mapping. *Eur J Radiol* 2015;84:1098-104.
  96. Matsubara H, Okazaki K, Takayama Y, Osaki K,

- Matsuo Y, Honda H, Iwamoto Y. Detection of early cartilage deterioration associated with meniscal tear using T<sub>1ρ</sub> mapping magnetic resonance imaging. *BMC Musculoskelet Disord* 2015;16:22.
97. Li X, Ma BC, Bolbos RI, Stahl R, Lozano J, Zuo J, Lin K, Link TM, Safran M, Majumdar S. Quantitative assessment of bone marrow edema pattern and overlying cartilage in knees with osteoarthritis and anterior cruciate ligament tear using MR imaging and spectroscopic imaging. *J Magn Reson Imaging* 2008;28:453-61.
  98. Zhao J, Li X, Bolbos RI, Link TM, Majumdar S. Longitudinal assessment of bone marrow edema-like lesions and cartilage degeneration in osteoarthritis using 3 T MR T<sub>1ρ</sub> quantification. *Skeletal Radiol* 2010;39:523-31.
  99. Bolbos RI, Ma CB, Link TM, Majumdar S, Li X. In vivo T<sub>1ρ</sub> quantitative assessment of knee cartilage after anterior cruciate ligament injury using 3 Tesla magnetic resonance imaging. *Invest Radiol* 2008;43:782-8.
  100. Li X, Kuo D, Theologis A, Carballido-Gamio J, Stehling C, Link TM, Ma CB, Majumdar S. Cartilage in anterior cruciate ligament-reconstructed knees: MR imaging T<sub>1ρ</sub> and T<sub>2</sub>--initial experience with 1-year follow-up. *Radiology* 2011;258:505-14.
  101. Theologis AA, Kuo D, Cheng J, Bolbos RI, Carballido-Gamio J, Ma CB, Li X. Evaluation of bone bruises and associated cartilage in anterior cruciate ligament-injured and -reconstructed knees using quantitative t(1ρ) magnetic resonance imaging: 1-year cohort study. *Arthroscopy* 2011;27:65-76.
  102. Klocke NF, Amendola A, Thedens DR, Williams GN, Luty CM, Martin JA, Pedersen DR. Comparison of T<sub>1ρ</sub>, dGEMRIC, and quantitative T<sub>2</sub> MRI in preoperative ACL rupture patients. *Acad Radiol* 2013;20:99-107.
  103. Su F, Hilton JF, Nardo L, Wu S, Liang F, Link TM, Ma CB, Li X. Cartilage morphology and T<sub>1ρ</sub> and T<sub>2</sub> quantification in ACL-reconstructed knees: a 2-year follow-up. *Osteoarthritis Cartilage* 2013;21:1058-67.
  104. Haughom B, Schairer W, Souza RB, Carpenter D, Ma CB, Li X. Abnormal tibiofemoral kinematics following ACL reconstruction are associated with early cartilage matrix degeneration measured by MRI T<sub>1ρ</sub>. *Knee* 2012;19:482-7.
  105. Zaid M, Lansdown D, Su F, Podoia V, Tufts L, Rizzo S, Souza RB, Li X, Ma CB. Abnormal tibial position is correlated to early degenerative changes one year following ACL reconstruction. *J Orthop Res* 2015;33:1079-86.
  106. Kumar D, Kothari A, Souza RB, Wu S, Benjamin Ma C, Li X. Frontal plane knee mechanics and medial cartilage MR relaxation times in individuals with ACL reconstruction: A pilot study. *Knee* 2014;21:881-5.
  107. Neidhart M, Müller-Ladner U, Frey W, Bosserhoff AK, Colombani PC, Frey-Rindova P, Hummel KM, Gay RE, Häuselmann H, Gay S. Increased serum levels of non-collagenous matrix proteins (cartilage oligomeric matrix protein and melanoma inhibitory activity) in marathon runners. *Osteoarthritis Cartilage* 2000;8:222-9.
  108. Vanwanseele B, Eckstein F, Knecht H, Spaepen A, Stüssi E. Longitudinal analysis of cartilage atrophy in the knees of patients with spinal cord injury. *Arthritis Rheum* 2003;48:3377-81.
  109. Hagiwara Y, Ando A, Chimoto E, Saijo Y, Ohmori-Matsuda K, Itoi E. Changes of articular cartilage after immobilization in a rat knee contracture model. *J Orthop Res* 2009;27:236-42.
  110. Luke AC, Stehling C, Stahl R, Li X, Kay T, Takamoto S, Ma B, Majumdar S, Link T. High-field magnetic resonance imaging assessment of articular cartilage before and after marathon running: does long-distance running lead to cartilage damage? *Am J Sports Med* 2010;38:2273-80.
  111. Stehling C, Luke A, Stahl R, Baum T, Joseph G, Pan J, Link TM. Meniscal T<sub>1ρ</sub> and T<sub>2</sub> measured with 3.0T MRI increases directly after running a marathon. *Skeletal Radiol* 2011;40:725-35.
  112. Peers SC, Maerz T, Baker EA, Shetty A, Xia Y, Puwal S, Marcantonio D, Keyes D, Guettler J. T<sub>1ρ</sub> magnetic resonance imaging for detection of early cartilage changes in knees of asymptomatic collegiate female impact and nonimpact athletes. *Clin J Sport Med* 2014;24:218-25.
  113. Wang L, Vieira RL, Rybak LD, Babb JS, Chang G, Krasnokutsky S, Abramson S, Regatte R. Relationship between knee alignment and T<sub>1ρ</sub> values of articular cartilage and menisci in patients with knee osteoarthritis. *Eur J Radiol* 2013;82:1946-52.
  114. Souza RB, Stehling C, Wyman BT, Hellio Le Graverand MP, Li X, Link TM, Majumdar S. The effects of acute loading on T<sub>1ρ</sub> and T<sub>2</sub> relaxation times of tibiofemoral articular cartilage. *Osteoarthritis Cartilage* 2010;18:1557-63.
  115. Subburaj K, Kumar D, Souza RB, Alizai H, Li X, Link TM, Majumdar S. The acute effect of running on knee articular cartilage and meniscus magnetic resonance relaxation times in young healthy adults. *Am J Sports Med* 2012;40:2134-41.
  116. Souza RB, Kumar D, Calixto N, Singh J, Schooler J, Subburaj K, Li X, Link TM, Majumdar S. Response of

- knee cartilage T1rho and T2 relaxation times to in vivo mechanical loading in individuals with and without knee osteoarthritis. *Osteoarthritis Cartilage* 2014;22:1367-76.
117. Zhu Y, Zhang Q, Liu Q, Wang YX, Liu X, Zheng H, Liang D, Yuan J. PANDA- T1ρ: Integrating principal component analysis and dictionary learning for fast T1ρ mapping. *Magn Reson Med* 2015;73:263-72.
  118. Pandit P, Rivoire J, King K, Li X. Accelerated T1ρ acquisition for knee cartilage quantification using compressed sensing and data-driven parallel imaging: A feasibility study. *Magn Reson Med* 2015. [Epub ahead of print]. doi: 10.1002/mrm.25702.
  119. Zhou Y, Pandit P, Pedoia V, Rivoire J, Wang Y, Liang D, Li X, Ying L. Accelerating t1ρ cartilage imaging using compressed sensing with iterative locally adapted support detection and JSENSE. *Magn Reson Med* 2015. [Epub ahead of print]. doi: 10.1002/mrm.25773.
  120. Pedoia V, Li X, Su F, Calixto N, Majumdar S. Voxel Based Relaxometry (T1ρ) of the Knee Articular Cartilage: A Comparison of Patterns of Biochemical Changes in Knees with Mild Osteoarthritis and Anterior Cruciate Ligament Injury. *J Magn Reson Imaging* 2015. (In press) doi: 10.1002/jmri.25065.
  121. Shan L, Zach C, Charles C, Niethammer M. Automatic atlas-based three-label cartilage segmentation from MR knee images. *Med Image Anal* 2014;18:1233-46.
  122. Carballido-Gamio J, Link TM, Li X, Han ET, Krug R, Ries MD, Majumdar S. Feasibility and reproducibility of relaxometry, morphometric, and geometrical measurements of the hip joint with magnetic resonance imaging at 3T. *J Magn Reson Imaging* 2008;28:227-35.
  123. Rakhra KS, Lattanzio PJ, Cárdenas-Blanco A, Cameron IG, Beaulé PE. Can T1-rho MRI detect acetabular cartilage degeneration in femoroacetabular impingement?: a pilot study. *J Bone Joint Surg Br* 2012;94:1187-92.
  124. Subburaj K, Valentinitich A, Dillon AB, Joseph GB, Li X, Link TM, Vail TP, Majumdar S. Regional variations in MR relaxation of hip joint cartilage in subjects with and without femoralacetabular impingement. *Magn Reson Imaging* 2013;31:1129-36.
  125. Wyatt C, Kumar D, Subburaj K, Lee S, Nardo L, Narayanan D, Lansdown D, Vail T, Link TM, Souza RB, Majumdar S. Cartilage T1ρ and T2 Relaxation Times in Patients With Mild-to-Moderate Radiographic Hip Osteoarthritis. *Arthritis Rheumatol* 2015;67:1548-56.
  126. McGuffin WS, Melkus G, Rakhra KS, Beaulé PE. Is the contralateral hip at risk in patients with unilateral symptomatic cam femoroacetabular impingement? A quantitative T1ρ MRI study. *Osteoarthritis Cartilage* 2015;23:1337-42.
  127. Al Maini M, Adelowo F, Al Saleh J, Al Weshahi Y, Burmester GR, Cutolo M, Flood J, March L, McDonald-Blumer H, Pile K, Pineda C, Thorne C, Kvien TK. The global challenges and opportunities in the practice of rheumatology: white paper by the World Forum on Rheumatic and Musculoskeletal Diseases. *Clin Rheumatol* 2015;34:819-29.
  128. Dagenais S, Caro J, Haldeman S. A systematic review of low back pain cost of illness studies in the United States and internationally. *Spine J* 2008;8:8-20.
  129. Fehlings MG, Tetreault L, Nater A, Choma T, Harrop J, Mroz T, Santaguida C, Smith JS. The Aging of the Global Population: The Changing Epidemiology of Disease and Spinal Disorders. *Neurosurgery* 2015;77 Suppl 4:S1-5.
  130. Miller JA, Schmatz C, Schultz AB. Lumbar disc degeneration: correlation with age, sex, and spine level in 600 autopsy specimens. *Spine (Phila Pa 1976)* 1988;13:173-8.
  131. Lebkowski WJ. Autopsy evaluation of the extent of degeneration of the lumbar intervertebral discs. *Pol Merkur Lekarski* 2002;13:188-90.
  132. Wang YX. Continued progression of lumbar disc degeneration in postmenopausal women. *Climacteric* 2015;18:435.
  133. Wang YX. Postmenopausal Chinese women show accelerated lumbar disc degeneration compared with Chmen. *Journal of Orthopaedic Translation* 2015;3:205-11.
  134. Johannessen W, Auerbach JD, Wheaton AJ, Kurji A, Borthakur A, Reddy R, Elliott DM. Assessment of human disc degeneration and proteoglycan content using T1rho-weighted magnetic resonance imaging. *Spine (Phila Pa 1976)* 2006;31:1253-7.
  135. Blumenkrantz G, Li X, Han ET, Newitt DC, Crane JC, Link TM, Majumdar S. A feasibility study of in vivo T1rho imaging of the intervertebral disc. *Magn Reson Imaging* 2006;24:1001-7.
  136. Griffith JF, Wang YX, Antonio GE, Choi KC, Yu A, Ahuja AT, Leung PC. Modified Pfirrmann grading system for lumbar intervertebral disc degeneration. *Spine (Phila Pa 1976)* 2007;32:E708-12.
  137. Pfirrmann CW, Metzendorf A, Zanetti M, Hodler J, Boos N. Magnetic resonance classification of lumbar intervertebral disc degeneration. *Spine (Phila Pa 1976)* 2001;26:1873-8.
  138. Wang YX, Griffith JF, Leung JC, Yuan J. Age related reduction of T1rho and T2 magnetic resonance relaxation

- times of lumbar intervertebral disc. *Quant Imaging Med Surg* 2014;4:259-64.
139. Vadalà G, Russo F, Battisti S, Stellato L, Martina F, Del Vescovo R, Giacalone A, Borthakur A, Zobel BB, Denaro V. Early intervertebral disc degeneration changes in asymptomatic weightlifters assessed by T<sub>1ρ</sub>-magnetic resonance imaging. *Spine (Phila Pa 1976)* 2014;39:1881-6.
  140. Brayda-Bruno M, Tibiletti M, Ito K, Fairbank J, Galbusera F, Zerbi A, Roberts S, Wachtel E, Merkher Y, Sivan SS. Advances in the diagnosis of degenerated lumbar discs and their possible clinical application. *Eur Spine J* 2014;23 Suppl 3:S315-23.
  141. Enean A, Palmer KT, Coggon D. Potential of magnetic resonance imaging findings to refine case definition for mechanical low back pain in epidemiological studies: a systematic review. *Spine (Phila Pa 1976)* 2011;36:160-9.
  142. Ogon I, Takebayashi T, Takashima H, Tanimoto K, Ida K, Yoshimoto M, Fujiwara H, Kubo T, Yamashita T. Analysis of chronic low back pain with magnetic resonance imaging T<sub>2</sub> mapping of lumbar intervertebral disc. *J Orthop Sci* 2015;20:295-301.
  143. Wang YX, Griffith JF. Biomedical imaging in translational orthopaedic research. *Journal of Orthopaedic Translation* 2015;3:157-9.
  144. Salzmänn GM, Erdle B, Porichis S, Uhl M, Ghanem N, Schmal H, Kubosch D, Südkamp NP, Niemeyer P. Long-term T<sub>2</sub> and Qualitative MRI Morphology After First-Generation Knee Autologous Chondrocyte Implantation: Cartilage Ultrastructure Is Not Correlated to Clinical or Qualitative MRI Outcome. *Am J Sports Med* 2014;42:1832-40.
  145. de Windt TS, Welsch GH, Brittberg M, Vonk L, Marlovits S, Trattng S, Saris DB, Blackman AJ, Smith MV, Flanigan DC, Matava MJ, Wright RW, Brophy RH. Correlation between magnetic resonance imaging and clinical outcomes after knee cartilage repair: letter to the editor. *Am J Sports Med* 2013;41:NP48-50.
  146. de Windt TS, Welsch GH, Brittberg M, Vonk LA, Marlovits S, Trattng S, Saris DB. Is magnetic resonance imaging reliable in predicting clinical outcome after articular cartilage repair of the knee? A systematic review and meta-analysis. *Am J Sports Med* 2013;41:1695-702.
  147. Yuan J, Wang YX. A general T<sub>1ρ</sub> relaxation model for spin-lock MRI using a rotary echo pulse. *Proc Intl Soc Mag Reson Med* 2011:124.
  148. Wang YX, Zhao F, Yuan J, Mok GS, Ahuja AT, Griffith JF. Accelerated T<sub>1ρ</sub> relaxation quantification in intervertebral disc using limited spin-lock times. *Quant Imaging Med Surg* 2013;3:54-8.
  149. Johnson CP, Thedens DR, Magnotta VA. Precision-guided sampling schedules for efficient T<sub>1ρ</sub> mapping. *J Magn Reson Imaging* 2015;41:242-50.
  150. Yuan J, Li Y, Zhao F, Chan Q, Ahuja AT, Wang YX. Quantification of T(1ρ) relaxation by using rotary echo spin-lock pulses in the presence of B(0) inhomogeneity. *Phys Med Biol* 2012;57:5003-16.
  151. Yuan J, Zhao F, Chan Q, Wang YX. Observation of bi-exponential T(1ρ) relaxation of in-vivo rat muscles at 3T. *Acta Radiol* 2012;53:675-81.
  152. Wang YX, Deng M. Medical imaging in new drug clinical development. *J Thorac Dis* 2010;2:245-52.
  153. Wang YX. Medical imaging in pharmaceutical clinical trials: what radiologists should know. *Clin Radiol* 2005;60:1051-7.
  154. Raastad J, Reiman M, Coeytaux R, Ledbetter L, Goode AP. The association between lumbar spine radiographic features and low back pain: a systematic review and meta-analysis. *Semin Arthritis Rheum* 2015;44:571-85.
  155. Blumenkrantz G, Zuo J, Li X, Kornak J, Link TM, Majumdar S. In vivo 3.0-tesla magnetic resonance T<sub>1ρ</sub> and T<sub>2</sub> relaxation mapping in subjects with intervertebral disc degeneration and clinical symptoms. *Magn Reson Med* 2010;63:1193-200.
  156. Müller-Lutz A, Schleich C, Pentang G, Schmitt B, Lanzman RS, Matuschke F, Wittsack HJ, Miese F. Age-dependency of glycosaminoglycan content in lumbar discs: A 3t gagcEST study. *J Magn Reson Imaging* 2015. [Epub ahead of print]. doi: 10.1002/jmri.24945.
  157. Wang YX, Mok G, Zhang D, Chen SZ, Yuan J. A comparison of three approaches for defining nucleus pulposus and annulus fibrosus on sagittal MR images. *Proc Intl Soc Mag Reson Med* 2015;23:1217.
  158. Wáng YX. Inner annulus fibrosus in non-degenerated intervertebral disc shows bright signal on T<sub>2</sub> weighted MR image. *Quant Imaging Med Surg* 2014;4:504.
  159. Mulligan KR, Ferland CE, Gawri R, Borthakur A, Haglund L, Ouellet JA. Axial T<sub>1ρ</sub> MRI as a diagnostic imaging modality to quantify proteoglycan concentration in degenerative disc disease. *Eur Spine J* 2015;24:2395-401.
  160. Crowell JM, Ransohoff DF, Kramer BS. Principles of cancer screening: lessons from history and study design issues. *Semin Oncol* 2010;37:202-15.
  161. Esserman L, Shieh Y, Thompson I. Rethinking screening for breast cancer and prostate cancer. *JAMA* 2009;302:1685-92.
  162. Marcus PM, Bergstralh EJ, Fagerstrom RM, Williams DE,

- Fontana R, Taylor WF, Prorok PC. Lung cancer mortality in the Mayo Lung Project: impact of extended follow-up. *J Natl Cancer Inst* 2000;92:1308-16.
163. Wáng YX, Gong JS, Loffroy R. On pancreatic cancer screening by magnetic resonance imaging with the recent evidence by Del Chiaro and colleagues. *Chin J Cancer Res* 2015;27:417-22.
164. Jordan CD, McWalter EJ, Monu UD, Watkins RD, Chen W, Bangerter NK, Hargreaves BA, Gold GE. Variability of CubeQuant T1 $\rho$ , quantitative DESS T2, and cones sodium MRI in knee cartilage. *Osteoarthritis Cartilage* 2014;22:1559-67.
165. Reddy R, Insko EK, Kaufman JH, Bolinger L, Kneeland JB, Leigh JS. MR Imaging of Articular Cartilage Under Spin-Locking. *Proc Annual Meeting ISMRM* 1995:1535.

**Cite this article as:** Wáng YX, Zhang Q, Li X, Chen W, Ahuja A, Yuan J. T $\rho$  magnetic resonance: basic physics principles and applications in knee and intervertebral disc imaging. *Quant Imaging Med Surg* 2015;5(6):858-885. doi: 10.3978/j.issn.2223-4292.2015.12.06